การสร้างฟิลาเมนต์ระดับนาโนเมตรของเงินโดยอิเล็กโทรไลต์แบบของแข็งของซิลเวอร์ซัลไฟด์สำหรับทิปเอ็นฮานซ์รามานสเปกโทรสโกปี

นางสาวพิชญา เฟื่อยมี

วิทยานิพนธ์นี้เป็นส่วนหนึ่งของการศึกษาตามหลักสูตรปริญญาวิทยาศาสตรมหาบัณฑิต
สาขาวิชาเคมี ภาควิชาเคมี
คณะวิทยาศาสตร์ จุฬาลงกรณ์มหาวิทยาลัย
ปีการศึกษา 2560

FABRICATION OF SILVER NANOFILAMENT BASED ON SILVER SULFIDE SOLID ELECTROLYTE FOR TIP-ENHANCED RAMAN SPECTROSCOPY

Miss Phichaya Fueaimi

A Thesis Submitted in Partial Fulfillment of the Requirements
for the Degree of Master of Science Program in Chemistry
Department of Chemistry
Faculty of Science
Chulalongkorn University
Academic Year 2017

Thesis Title	FABRICATION OF SILVER NANOFILAMENT BASED ON SILVER SULFIDE SOLID ELECTROLYTE FOR TIP-ENHANCED RAMAN SPECTROSCOPY
By	Miss Phichaya Fueaimi
Field of Study	Chemistry
Thesis Advisor	Pannee Leeladee, Ph.D.
Thesis Co-Advisor	Professor Thawatchai Tuntulani, Ph.D. Chaweewan Sapcharoenkun, Ph.D.

Accepted by the Faculty of Science, Chulalongkorn University in Partial Fulfillment of the Requirements for the Master's Degree

.....Dean of the Faculty of Science
(Professor Polkit Sangvanich, Ph.D.)

THESIS COMMITTEE

.....Chairman
(Associate Professor Vudhichai Parasuk, Ph.D.)

.....Thesis Advisor
(Pannee Leeladee, Ph.D.)

.....Thesis Co-Advisor
(Professor Thawatchai Tuntulani, Ph.D.)

.....Thesis Co-Advisor
(Chaweewan Sapcharoenkun, Ph.D.)

.....Examiner
(Assistant Professor Prompong Pienpinijtham, Ph.D.)

.....External Examiner
(Annop Klamchuen, Ph.D.)

พิชญา เฟื่อยมี : การสร้างฟิลาเมนต์ระดับนาโนเมตรของเงินโดยอิเล็กโทรไลต์แบบของแข็งของซิลเวอร์ซัลไฟด์สำหรับทิปเอ็นฮานซ์รามานสเปกโทรสโกปี (FABRICATION OF SILVER NANOFILAMENT BASED ON SILVER SULFIDE SOLID ELECTROLYTE FOR TIP-ENHANCED RAMAN SPECTROSCOPY) อ.ที่ปรึกษาวิทยานิพนธ์หลัก: ดร.พรรณี ลีลาดี, อ.ที่ปรึกษาวิทยานิพนธ์ร่วม: ศ. ดร.ธวัชชัย ตันฑุลานิ, ดร.ฉวีวรรณ ทรัพย์เจริญกุล, 55 หน้า.

เทคนิคทิปเอ็นฮานซ์รามานสเปกโทรสโกปี (TERS) เป็นหนึ่งในเทคนิคพื้นฐานที่สำคัญในการศึกษาในระดับนาโนซึ่งเป็นการศึกษาด้านพื้นผิวและองค์ประกอบทางเคมี โดยอาศัยหลักการทำงานร่วมกันของกล้องจุลทรรศน์แรงอะตอมและเทคนิครามานสเปกโทรสโกปี ซึ่งหัวใจสำคัญของเทคนิค TERS คือเข็มโดยจะต้องขยายสัญญาณรามานที่สูง และให้ความละเอียดภาพที่สูงด้วย ปัจจุบันมีหลากหลายวิธีในการทำเข็มเพื่อใช้สำหรับ TERS ตัวอย่างเช่น การระเหยโดยใช้ความร้อน และ การกัดทางเคมีไฟฟ้า แต่เทคนิคเหล่านี้มีข้อจำกัดทางด้านการจัดเรียงตัวที่ไม่เป็นระเบียบของอนุภาคนาโนที่ปลายเข็ม และสามารถทำได้ในปริมาณไม่มาก อีกทั้งยังยากต่อการทำเข็มซ้ำให้มีลักษณะเดิม ดังนั้นในงานวิจัยนี้จึงเสนอวิธีการใหม่ที่ง่ายต่อการพัฒนา และสามารถควบคุมลักษณะของเข็มสำหรับ TERS โดยการเตรียมเส้นลวดเงินในระดับนาโนเมตร (Ag NFs) บนฐานรองรับที่มีการเคลือบด้วยเบต้าซิลเวอร์ซัลไฟด์ (β-Ag_2S) ซึ่งทำหน้าที่เป็นอิเล็กโทรไลต์แบบของแข็ง จากการศึกษาพบว่าสภาวะเหมาะสมในการสังเคราะห์ β-Ag_2S ด้วยวิธีการเคลือบอาบสารเคมีที่ความเข้มข้นของสารละลายโซเดียมซัลไฟด์ที่ 0.5 mM เป็นระยะเวลา 6 ชั่วโมงและ pH 8.45. และทำการสังเคราะห์เส้นลวดเงินในระดับนาโนเมตรด้วยเทคนิคการฉายลำอิเล็กตรอน โดยใช้อัตราเร่งที่ 20 kV และเวลาในการฉาย 10 นาที สามารถสังเคราะห์เส้นลวดเงินในระดับนาโนเมตรที่มีความหนาแน่นเท่ากับ 5.93 x 10^9 เส้น/ตารางเซนติเมตร และเส้นลวดเงินมีความยาวที่ 0.46 ± 0.04 ไมโครเมตร เมื่อศึกษาการเพิ่มสัญญาณรามานของเมทิลีนบลูโดยแสงสีเขียวที่ความยาวคลื่น 532 นาโนเมตร โดยใช้เส้นลวดเงินในระดับนาโนเมตรบนแผ่น Si เป็นฐานรองรับ พบว่ามีค่าขยายสัญญาณเท่ากับ 1.57x10^6 นอกจากนี้ยังสามารถตรวจวัดความเข้มข้นที่น้อยที่สุดของเมทิลีนบลูได้ที่ 10 nM และ เมื่อใช้เส้นลวดเงินในระดับนาโนเมตรบนเข็ม AFM เป็นฐานรองรับพบว่ามีค่าการเพิ่มสัญญาณรามานของเมทิลีนบลูเท่ากับ 4.27 x 10^4

ภาควิชา	เคมี	ลายมือชื่อนิสิต .....
สาขาวิชา	เคมี	ลายมือชื่อ อ.ที่ปรึกษาหลัก .....
ปีการศึกษา	2560	ลายมือชื่อ อ.ที่ปรึกษาร่วม .....
		ลายมือชื่อ อ.ที่ปรึกษาร่วม .....

5772078923 : MAJOR CHEMISTRY

KEYWORDS: SILVER / SILVER SULFIDE / SOLID ELECTROLYTE / TERS / ELECTRON IRRADIATION / METHYLENE BLUE

PHICHAYA FUEAIMI: FABRICATION OF SILVER NANOFILAMENT BASED ON SILVER SULFIDE SOLID ELECTROLYTE FOR TIP-ENHANCED RAMAN SPECTROSCOPY. ADVISOR: PANNEE LEELADEE, Ph. D. , CO-ADVISOR: PROF. THAWATCHAI TUNTULANI, Ph.D., CHAWEEWAN SAPCHAROENKUN, Ph.D., 55 pp.

Surface science analysis is the crucial fundamental of nanoscale study. The techniques combined morphological and compositional study on the surface are the promising technique. Tip-enhanced Raman spectroscopy (TERS) is the coupling of atomic force microscopy (AFM) and Raman spectroscopy which give the 3D- images and bonding information in ambient conditions. Furthermore, TERS tip is an ideal tool for the high enhancement and spatial resolution. Nowadays, TERS tip fabrication is still challenged. There are three main challenges that are high enhancement factor of the TERS tip, reproducibility of the tip and in-depth understanding of TERS process. We introduce the simple method for fabrication of silver nanofilaments (Ag NFs) based on β-silver sulfide (β-Ag_2S) solid electrolyte for TERS. The highest amount of β-Ag_2S was synthesized from 0.5 mM for 6 hours at pH 8.45 by chemical bath deposition (CBD). The highest density and length were achieved from 20 kV of accelerated voltage and 10 minutes by electron beam irradiation. The highest density and length of Ag NFs were found to be 5.93×10^9 NF/cm^2 and 0.46 ± 0.04 μm, respectively. The Ag NFs performance has been investigated by using Ag NFs as surface enhanced Raman spectroscopy (SERS) substrates. Methylene blue (MB) adsorbed on Ag NFs substrate with green laser (532 nm) and the maximum SERS enhancement factor of 1.57×10^6 was achieved. The limit of detection of MB obtained from Ag NFs substrate was found to be at 10 nM. The highest enhancement factor of 4.27×10^4 of MB absorb on Ag NFs TERS tip performed as SERS substrate was achieved.

Department:	Chemistry	Student's Signature	.....
Field of Study:	Chemistry	Advisor's Signature	.....
Academic Year:	2017	Co-Advisor's Signature	.....
		Co-Advisor's Signature	.....

ACKNOWLEDGEMENTS

I am grateful to my research advisor, Dr. Pannee Leeladee, for her providing any helpful suggestions throughout this research. In addition, I would like to thank my co- advisors, Dr. Chaweewan Sapcharoenkun and Professor Dr. Thawatchai Tuntulani, for the opportunity to work in the high performance laboratory, teaching and assisting in material characterizations and valuable comments. I would like to thank Dr. Annop Klamchuen and his research group for essential skills during my research. I also would like to thank and pay my respect to Associate Professor Dr. Vudthichai Parasuk and Assistant Professor Dr. Prompong Pienpinijtham for their valuable advices and comments as thesis committee.

Furthermore, this work was financially supported by National Nanotechnology Center (NANOTEC) from the National Science and Technology Development Agency (NSTDA) and the 90th Anniversary of Chulalongkorn University Scholarship under contract number as GCUGR1125603062M (No. 58). We also acknowledge the scholarship supported by the Thailand Graduate Institute of Science and Technology (TGIST) under contract number as SCA-CO-2559-2317-TH.

Finally, I would like to thank all members of my family. They have continued to give me an assistance, kindness and encouragement unconditionally in order to gain this accomplishment.

CONTENTS

Page

Page

Page

LIST OF FIGURES

CHAPTER I
INTRODUCTION

Surface science is devoted to study the fundamental of chemical and physical phenomena occurring at a wide range of surfaces and interfaces. Morphology and composition are two major analytical aspects which have been studied in this field. For the former aspect, the microscopic techniques such as scanning electron microscopy (SEM), transmission electron microscopy (TEM), and atomic force microscopy (AFM) are normally used to investigate a sample surface. While the spectroscopic techniques, for example, Raman spectroscopy, Infrared spectroscopy and X-ray diffraction (XRD) are commonly employed for studying the chemical composition.

Raman spectroscopy, a non-destructive and non-invasive technique, is one of the most common vibrational spectroscopic techniques used for the structural characterization in a broad range of analytical sample [1-3]. Raman spectroscopy is based on scattering of radiation on analytical sample. A very small percentage of scattering light is inelastic scattering or Raman scattered light. Due to the Raman scattered light is extremely weak of process that only one in 10^6-10^8 photon emission. However, one of the major disadvantages of this method is the intrinsic low intensity of Raman signals in many organic compounds and biomolecules [4, 5]. To overcome this limitation, several studies have developed a novel method known as surface enhanced Raman spectroscopy or SERS.

The discovery of SERS over 30 years ago provides an opportunity to overcome the limitation of Raman and can improve the weak Raman intensity even at low concentrations due to its significant enhancement effects [6, 7]. SERS provides greatly enhanced Raman signal from Raman-active analytical molecules that have been adsorbed onto specially prepared noble metal surfaces such as gold, silicon, silver and copper [8-11]. SERS offers an increase in the Raman intensity on orders of magnitudes

(10^6 or more) [12-16]. In addition, the resolution of SERS is limited by Abbé diffraction limit (equation 1). This is the diffraction-limited resolution of an optical system.

$$d \sim \lambda/NA \qquad (1)$$

where: d = resolution

λ = wavelength of imaging radiation

NA = numerical aperture

The resolution is depending on the wavelength of laser source. In visible light, the limit of resolution found about 200 nm. To overcome this limitation, several studies have developed a novel method known as Tip-enhanced Raman spectroscopy or TERS [17-19].

TERS combines the advantage of SERS based on the similar principles with the high spatial resolution of scanning probe microscopy (SPM). In TERS, the excitation of the LSPR produces at the sharp apex tip, which is located in the proximity region of a focused laser beam. Hence, the tip apex acts as an optical nanoantenna that enhances both incident and scattered light [20, 21]. The local confinement of the electric field at the tip apex enhances the Raman intensity. Therefore, the shape and size of the tip apex play an important role for the enhancement and the spatial resolution of TERS. [22-24]

In recent years, the topic of TERS tip fabrication is of interest in many research groups [25]. Thermal evaporation in vacuum is one of the most common methods for preparing TERS tips [19]. However, the yield of TERS tips enhancing the Raman signal is relatively low due to the random nucleation and growth process of metal nanoparticles around the tip apex. An electrochemical etching method is another option to produce TERS tips. Williams and Roy used hydrochloric acid as the etchant for etching gold wires [26]. The gold tips have the radius smaller than 10 nm. However, the utilization of TERS has been hampered by the tip-yield and reproducibility. Many researcher tried to operate TERS tips in ultrahigh-vacuum (UHV) environments for prevent degradation of the tip but the professional operating was challenged [27, 28].

To overcome the above mentioned problems, an atomic switch provides an opportunity to fabricate TERS tips. Nayark *et al.* reported the formation and annihilation of a Ag atomic bridge using a solid-electrochemical reaction in a nanogap between Ag_2S solid-electrolyte electrode and a counter platinum electrode [29]. The switching time of a Ag_2S atomic switch as a function of bias voltage and temperature was studied. It was found that the reduction for the Ag atom precipitation is the rate-limiting step at lower bias voltage. Therefore, this method can be used to control the size of the Ag nanowire by adjusting the bias voltage.

1.1. Concept of this study

In this work, a novel and easy method to fabricate TERS tips in a controllable manner was developed. Ag NFs on the AFM tip used as TERS tips were fabricated by using electron irradiation method based on β-Ag_2S solid electrolyte. This work was divided into three parts. In the first part, β-Ag_2S solid electrolytes were fabricated employing the chemical bath deposition. The optimal conditions for β-Ag_2S fabrication was investigated and then the fabricated β-Ag_2S was characterized by various techniques including XRD, AFM, UV-visible spectroscopy and Raman spectroscopy. Then, Ag NFs were constructed by the electron irradiation process. The irradiated conditions including accelerated voltage and irradiation time were studied to obtain the proper Ag NFs structures. The second part focused on the modification of Ag NFs on the AFM tips using the optimized conditions obtained from the first part. In the final part, the performance of Ag NFs will be studied to investigate the Raman enhancement and scanning probe as TERS activities on methylene blue (MB) sample.

1.2. Objectives

1.1.1 Fabrication and characterization of Ag NFs based on **β**-Ag_2S solid electrolytes by electron irradiation process

1.1.2 Fabrication and characterization of TERS tips by modification of Ag NFs on Ag_2S-coated AFM tips

1.1.3 Study the performance of TERS tips on MB sample

CHAPTER II

THEORETICAL BACKGROUND AND LITERATURE REVIEW

2.1. Silver/ silver sulfide heterostructure (Ag/Ag_2S)

Silver (Ag) nanomaterials have been increasingly used in many applications, for example, antibacteria, bio-sensing, electronic, photocatalyst [30] due to their unique chemical and physical properties. In the last decades, Ag nanomaterials have also been employed as the SERS substrates [16, 31, 32] and TERS tip [25, 33]. The gap distance of Ag nanoparticle on substrate give the different enhancement in SERS [34]. In addition, the different shapes of Ag nanoparticles give the absorption and scattering at different wavelengths and also different electric filed distributions. Especially, Ag nanowire shows the highest electric field distribution mainly at the nanowire ends, or "hot spots" [35] as shown in Figure 2.1. Ag nanowire can act as optical antennas because the free electrons of Ag are in resonance with the incident light. So Ag nanowire is the interesting material for the enhancement of photoresponsive processes.

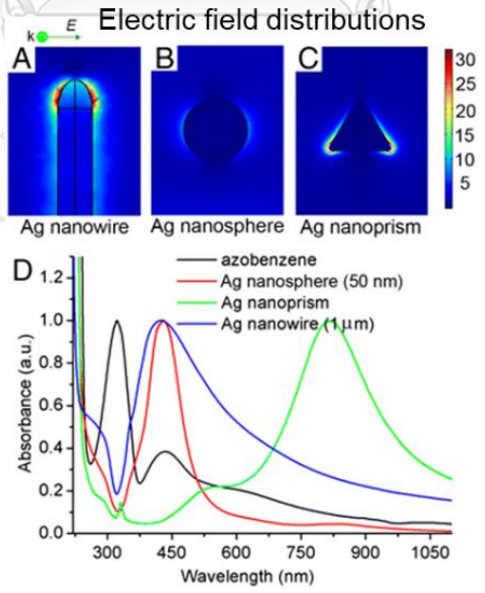

Figure 2.1 Electric field distributions at wavelength of 350 nm (|E|2) calculated for (A) Ag nanowire (1 μm); (B) Ag nanosphere (50 nm); (C) Ag nanoprism (50 nm). (D) Extinction spectra of Ag nanostructures and absorption spectra of azobenzene [35]

Silver sulfide (Ag_2S) is one of the excellent metal chalcogenides as a semiconducting sulfide due to its unique physical and chemical properties with high ion conductivity and thermal stability [36, 37]. Ag_2S solid electrolytes consist of 3 phases in different structures including **α**-Ag_2S (monoclinic), **β**-Ag_2S (body center cubic) and **γ**-Ag_2S (face center cubic). It is thought that **α**-Ag_2S is stoichiometric whereas **β**-Ag_2S and **γ**-Ag_2S are nonstoichiometric comprising of a small deficiency or small excess of silver [38]. During the last two decades, the Ag/Ag_2S heteromaterials have become the promising substance because of the coupling of quantum confinement leading to the plasmon-enhanced emission or absorption. An extensive number of methods have been reported for the synthesis of Ag/Ag_2S heteromaterials with different particle sizes, shapes and surface properties [30, 39]. However, Ag_2S phases have an effect on the preparation of Ag nanoprotrusion from solid electrochemical reaction**.** In 2014, Tanaka *et al.* reported a chemical bath deposition **(**CBD**)** used for low**-**cost fabrication of Ag_2S thin films **[**40**]** as shown in Figure 2**.**2**.** Ag thin films on SiO_2 substrates were dipped into 0.01% Na_2S aqueous solution. From the result, at the beginning **α**-Ag_2S (monoclinic) was precipitated for the dipping time shorter than 12 h, then **β**-Ag_2S (cubic) was precipitated after 12-h dipping time (Figure 6). Moreover, the Ag nanofilaments (Ag NFs) were grown by electron irradiation on **β**-Ag_2S (cubic) only.

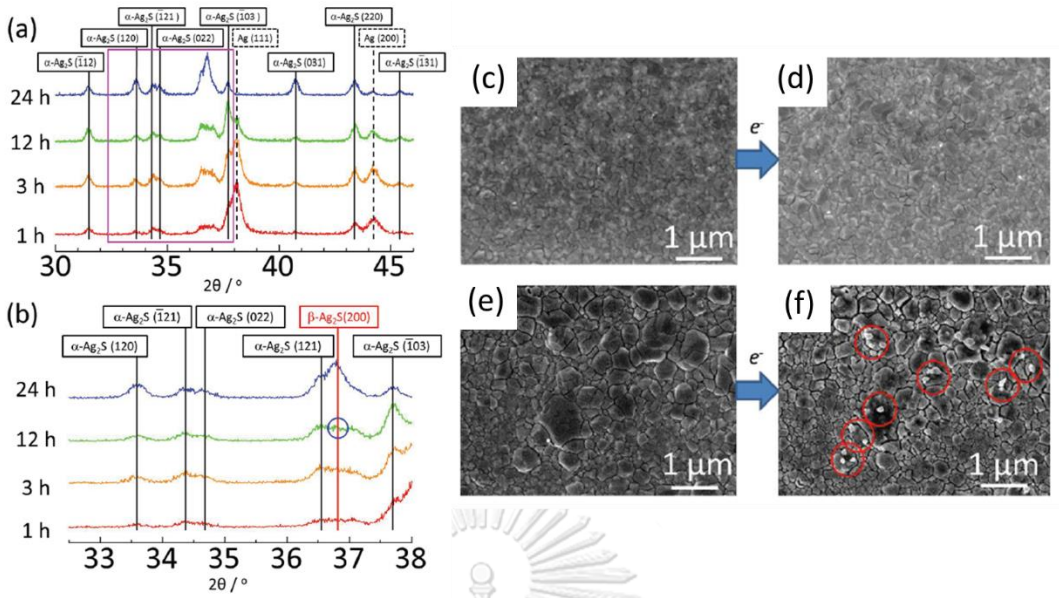

Figure 2.2 (a) Profile of GIXRD at **α** = 0:5° Solid black lines and dashed lines show peak positions of **α**-Ag_2S and Ag, respectively. (b) Magnified profiles in pink box in (a). The red and black lines show peak positions of **α**-Ag_2S and **β**-Ag_2S, respectively. After dipping for approximately 12 h, peaks from cubic **β**-Ag_2S started to be appeared (indicated by blue circle). (c) Ag surface dipped in 0.01%-Na_2S aqueous solution for 3 h. (d) Electron beam was irradiated to the same area of (a). No Ag wires were grown. (e) Ag surface dipped in 0.01%-Na_2S aqueous solution for 12 h. (f) Electron beam was irradiated to the same area of (e). Ag wires were grown by the reduction of Ag_2S. The electron beam was irradiated to (c) and (e) under the same condition [40].

The nanostructure of Ag_2S has been studied extensively in the past two decades, however, there is currently study on the phase transition of Ag_2S. Sadovnikov and co-worker studied the **α**-Ag_2S (acanthite)–**β**-Ag_2S (argentite) phase transformation in nanocrystalline and coarse-crystalline powders of silver sulfide via in situ by the scanning electron microscopy method in real-time [41]. They found that the formation of argentite crystals takes place on the surface of acanthite particles as a result of electron beam heating. The electron beam intensity is not sufficient for heating a thicker acanthite layer up to the transformation temperature ~450 K.

The different concentrations of initial sulfide reactant play a key role on the number of sulfide nuclei and the rate of deposition [42]. There are several methods used to fabricate Ag NFs including solid electrochemical reaction induced by a scanning tunneling microscope (STM) and electron beam irradiation. Terabe *et al.* developed a nanostructuring method using the solid electrochemical effects induced by the STM [43]. An ionic/electronic mixed conductor was used as the material for STM tip. To fabricate the Ag nanostructures, an oxidation/reduction reaction of mobile metal ions in the mixed conductor tip was used. It was shown that a nanoscale Ag nanoparticle was fabricated at the tip apex of the Ag_2S tip when a negative bias was applied to the sample with controllable rate. Motte *et al.* investigated the nucleation of Ag atom takes place on the surface of the Ag_2S nanocrystal by electron beam irradiation in TEM [39]. It was indicated that the Ag_2S acts as a center for subsequent reduction of Ag^+ ions. In their case, the proportions in the composite $(Ag)_x(Ag_2S)_y$ material can be modulated by electron beam irradiation. Therefore, the electron beam irradiation has shown to be a promising method to fabricate Ag NFs on the AFM tips used as TERS tips due to its short reaction time, simple operation, and the absence of chemical residues after the reaction.

2.2. Raman spectroscopy

Raman spectroscopy is the primary chemical characterization used to provide information on molecular vibrations. When the sample was irradiated by incident light source of Raman spectroscopy, sample molecule is vibrated. The vibration of molecule effects the scattered light of incident light source. Most of the scattering light is elastic scattering light or Rayleigh scattered light which no changing in energy from incident light. Raman signals can be obtained from the emission of photons (inelastic scattering) that different energy from the incident light source as shown in Figure 2.1. The Raman signal was obtained one in ten-millions of incident photons. So Raman spectroscopy produced weak signals and required a large amount of analytical sample to produce detectable signals.

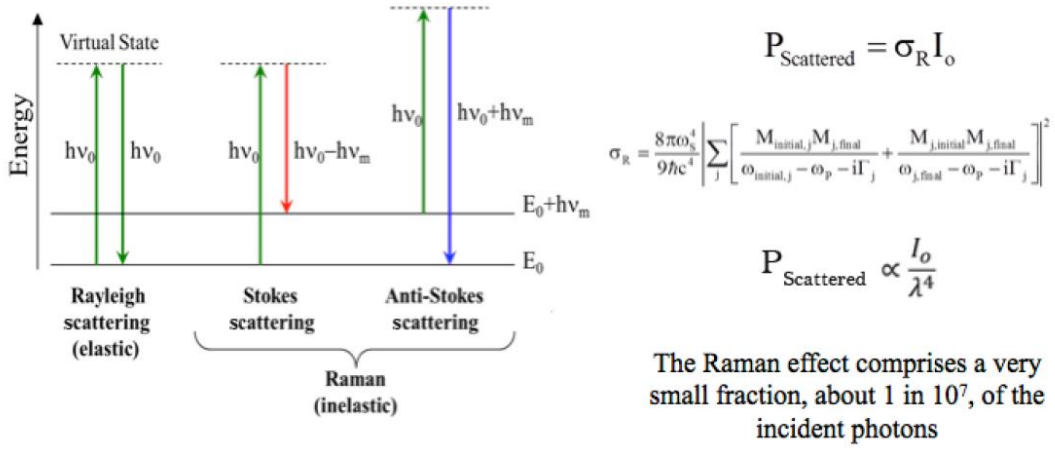

Figure 2.3. Diagram of scattered process in Raman spectroscopy and a quantum energy of diagram.

2.3. SERS enhancement mechanism

There are two primary enhancement mechanisms of SERS including electromagnetic (EM) and chemical enhancements (CE) [44, 45]. EM effect is dominant and dependent on the metal surface's roughness features on the order of tens of nanometers which is smaller than the wavelength of the incident beam. This small feature of the metal surface allows the excitation of the surface plasmon to be localized on the metal particle so-called localized surface plasmon resonance (LSPR) as shown in Figure 1. The Conduction electrons in metal or metal-like nanomaterials can be excited by incident light to oscillate collectively at metal/dielectric interfaces. The collective oscillating mode of electrons and the nanomaterials that support them are referred to as surface plasmons and plasmonic materials, respectively. CE involves molecular charge-transfer interactions between the adsorbed molecule and the metal surface. However, in SERS the high spatial resolution and sensitivity are still a great challenge since they are dependent on the excitation wavelength, and the focusing properties of the used microscopic objective.

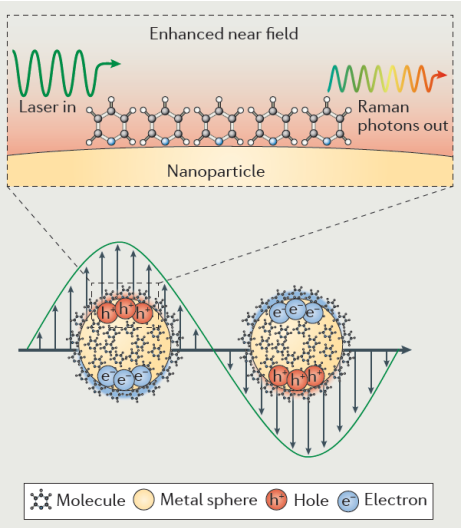

Figure 2.4. The localized surface plasmon resonance mechanism of metal sphere exciting by laser source

2.4. TERS tips fabrication.

The TERS tips fabrication relies on several parameters related to the technical requirements of the scanning probe methodology with nanoscale precision [46]. Top-down process is one of TERS the tip fabrication. Electrochemical etching is the method most used for STM-TERS tip construction (Figure 7a). Ag or Au wire was etched by the etchant and produced a tip with a radius of curvature at the apex of a few tens of nanometers. To electrochemically etch tips, the Ag act as anode and Pt act as cathode [47, 48]. However, the utilization of TERS has been hampered by the tip-yield and reproducibility. A template-stripping fabrication technique was used to fabricate the high-quality, uniform, ultra-sharp (10 nm) metallic probes suitable for single-molecule imaging. [49] The tip geometry is shown in Figure 7b. But the construction of template was complex and the several chemical waste was achieved [49]. The physical vapor deposition is the common for commercially AFM tips [50]. However, the yield of TERS tips enhancing the Raman signal is relatively low due to the random nucleation and growth process of metal nanoparticles around the tip apex. (Figure 7c) Moreover, the roughness of tip was a disadvantage of the incident laser focusing at the tip apex.

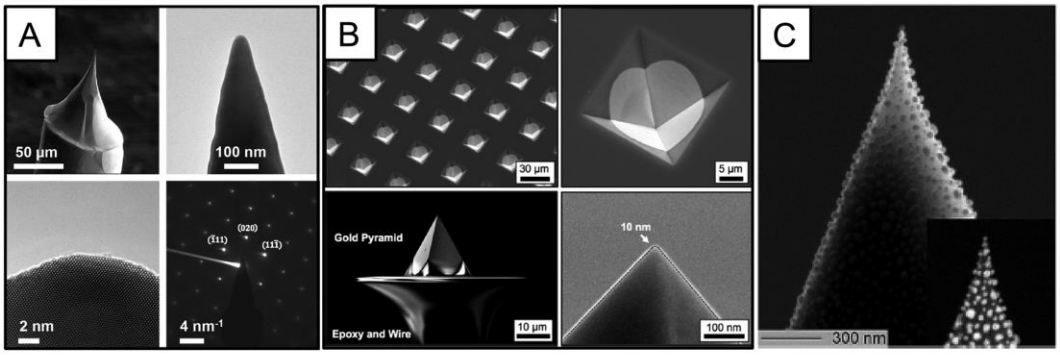

Figure 2.5 Sampling of tip fabrication methods using top-down (A) Au tip fabricated by electrochemical etching and characterized by SEM (top left), TEM (top right and bottom left), and electron diffraction (bottom right). (B) Massively parallel microfabrication of Au tips characterized by SEM. (C) Ag deposition on a silicon AFM cantilever with a single nanoparticle at its apex, as evidenced by SEM.

CHAPTER III

EXPERIMENTAL

3.1. General Procedure

3.1.1. Materials

Sodium sulfide nonahydrate ($Na_2S•9H_2O$) (98%) were manufactured by Carlo Erba Reagenti Carlo Erba Reagenti. Methylene blue ($C_{16}H_{18}ClN_3S$) (95% Conc. Nitric acid (HNO_3), Sodium hydroxide (NaOH) were obtained from Sigma-Aldrich. Acetone ($(CH_3)_2CO$) (95%), Ethyl alcohol (C_2H_5OH) (95%) were manufactured by Merck. All Chemicals and solvents are analytical grade used without further purification. The p-type (B-doped) Si (100) wafer were purchased from Semiconductor Wafer, Inc., Taiwan. The Ag and Ti targets (99.99%) with 3-inch diameter and 0.25-inch thickness were manufactured by Kurt J. Lesker Company. The Ar (99.999%), N_2 (95.5%) gases were obtained from Praxair Co., Ltd. and S.I. Technology Co., Ltd., respectively. Noncontact Si tips (VIT_P/IR) were purchased from TipsNano Co. with a tip radius of 10 nm and thickness of the chip is 0.3 mm.

3.1.2. Instruments

Sputtering machine UNIVEX 350) with thickness monitor INFICON SQM-160) manufactured by Oerlikon, Germany as shown in Figure 3.1. was used to prepare Ag thin films. Ultrasonic cleaner (Citizen Aczet Pvt. Ltd., India) was used to clean Si (100) substrate before sputtering by using acetone, water and ethanol, respectively. The crystal orientation of Ag and Ag_2S thin films was investigated by X-ray diffractometer (XRD, D8 ADVANCE), manufactured by Bruker. Moreover, the morphology of Ag and Ag_2S thin films was examined by field emission scanning electron microscope (FESEM, Versa 3D DualBeam), manufactured by Field Emission Inc. and atomic force microscope (AFM, Seiko SPA400), manufactured by Seiko Instruments, Inc. The chemical composition of Ag and Ag_2S thin films was determined by UV-visible spectrometer (UV-Vis, Cary4000), manufactured by Agilent Technologies, and Confocal Raman

spectroscopy (NT-MDT NTEGRA SPECTRA) equipped wtih IX71 Olympus microscope with 100x objective lens. The pH of solution was detected by pH meter (HI 98103) manufactured by Hanna instruments, Inc.

Figure 3.1. Sputtering machine

3.2. Synthesis

3.2.1. Synthesis of Ag Thin films

The ion Sputtering is a physical method used to deposit materials on a surface of substrate via the positive ions from gaseous plasma such as Ar gas were accelerated to bombard a solid target material in a high vacuum chamber. A voltage is placed between target and substrate which ionizes argon atom and create plasma, hot gas-like phase consisting of ions and electrons, in the chamber. This plasma is known as a glow discharged due to the light emitted. These argon ions are accelerated to the cathode target. The forceful collision of these ions onto the target ejects target atoms into the chamber. These ejected atoms reach the substrate and start to form into a film. More atoms coalesce on the substrate. Consequently, they begin to bind to each other at the molecular level, forming a tightly bound atomic layer. One or more layers of such atoms can be created and will depend on the sputtering time, allowing for production of precise layered thin film structures. Electrons released during argon ionization accelerate to anode substrate, which subsequently collide with addition

argon atoms creating more ions and electrons in process. The progress has been continued cycle by cycle.

Ag thin films were fabricated on silicon (Si) (100) and AFM tips by using RF reactive magnetron sputtering deposition technique. A 3-inch diameter with a 0.25-inch thickness of Ag target was used as a sputtering target. The Si (100) substrates were cleaned with acetone, ethyl alcohol and deionized water, respectively for 15 minutes each and then dried with the nitrogen gas. The samples were transferred to the high vacuum chamber for thin film deposition. The holder substrate was rotated by motor with rotation speed of 10 rpm. When a base pressure was reached to 5.0 $\times 10^{-6}$ mbar, a constant flow of high purity of Ar gas was introduced into the chamber at 20 sccm by mass flow meters. The RF power and working pressure of Ti were used at 120 watt and 7.5×10^{-3} mbar, respectively. The 20 nm thick of Ti was used as an adhesive layer. The RF was turned off and Ar flow rate was increased to 80 sccm. The RF power of Ag were used at 100 watt and the Ar flow rate was gradually decrease to 20 sccm. The working pressure was used at 7.5×10^{-3} mbar. The thickness of Ag thin films was 100 nm, which were measured by thickness monitor. The crystal orientation of Ag thin films was characterized by XRD (Cu K_{α}) recorded the 2θ from 20 to 80 degree with the step of 0.5 degree per minute. The current of X-ray was generated with the potential of 40 mA and 40 kV. The ratio of Ag (111)/ (200) was calculated from the ratio of peak intensity of each crystal plane. Moreover, UV-vis spectrometer was used to determine %T of Ag thin films with wavelength scan rage of 200-1500 nm. FE-SEM was used to characterized surface morphology of Ag thin films. The accelerated voltage was used at 20 kV and EDS also used to investigate the layers of each element of Ag thin film with 30-40% dead time. AFM were also employed to investigate the morphology of Ag thin films.

3.2.2. Synthesis of Ag Tips

The preparation of Ag tips was used the suitable condition from previous studying in Ag thin films. The AFM tips was used as substrate for sputtering technique. The thickness of Ag was varied from 100, 200 and 400 nm. FE-SEM and EDS mapping were used to morphologic and chemical characterizations.

3.2.3. Synthesis of β-Ag_2S Thin films

3.2.3.1. Preliminary study

Follow the procedure of Tanaka [40], a wet chemical process was used to low cost sulfurization. Each of 100 nm thick Ag thin films were dipped into 0.1 M of Na_2S for 6 h in duran bottles. Temperature of each bottle was varied from 120, 90, 50 °c and room temperature.

3.2.3.2. Effect of high Na_2S concentration and dipping time on β-Ag_2S synthesis

The 100 nm thick Ag thin films were dipped into an aqueous solution of Na_2S for sulfurization. The concentration of Na_2S and dipping time were varied from 10, 20, 30, 50, and 80 mM and 3, 6, and 12 hours, respectively at room temperature. The synthesis procedures are listed consequently as follows;

1. Na_2S solution was initially prepared by dissolving $Na_2S•9H_2O$ at concentration range between 10, 20, 30, 50 and 80 mM in deionized water.
2. Each Ag thin film was dipped into 5 ml of different concentration of Na_2S solutions in a sealed Duran bottle.
3. Each bottle was used dipping time for 3, 6, 12 and 24 h. at room temperature.
4. Finally, the Ag_2S thin films was washed with deionized water and dried in N_2 gas.

3.2.3.3. Effect of low Na_2S concentration and dipping time on β-Ag_2S synthesis

The Na_2S concentration was varied from 0.5, 2, 5, 10 mM. The dipping time was varied from 3, 6, 12 and 24 h. The procedure is the same from previous experiment. The reaction mechanism is proposed according to the following reactions:

$Na_2S(s) + H_2O(l) \rightarrow NaHS(aq) + NaOH(aq)$ (1)

$2Ag(s) + NaHS(aq) \rightarrow Ag_2S(s) + NaH(aq)$ (2)

Oxidation: $2Ag \rightarrow 2Ag^+ + 2e^-$ (3)

Reduction: $NaHS + 2e^- \rightarrow NaH + S^{2-}$ (4)

Conc. HNO_3 and Conc. NaOH were added into Na_2S solution to prepare a wide range of pH between 3.82 and 11.7. XRD, UV-Vis Spectrometer and confocal Raman spectrometer were used for the compositional analysis. The microscopic confocal Raman spectroscope using a laser beam with an excitation wavelength of 532 nm and charge-couple device (CCD) with a resolution of 4 cm^{-1}. The roughness of the surface was measured using tapping mode AFM. FESEM was used to compare the surface morphology of Ag_2S thin films which were obtained from different concentrations and dipping time.

3.2.4. Synthesis of Ag_2S tips

The Ag_2S tips were prepared by using the suitable conditions from Ag_2S thin films study. The Ag_2S were characterized by FE-SEM and EDS mapping for surface and chemical studies.

3.2.5. Synthesis of Ag nanofilaments (Ag NFs)

3.2.5.1. Electron beam irradiation

The Ag NFs were fabricated by electron irradiation from SEM. Each Ag_2S thin films prepared from different conditions of Na_2S concentration and dipping time were used to Ag NFs studied. Accelerated voltages used were 5, 10 and 20 kV and irradiation time were investigated at 1, 5 and 10 minutes on Ag_2S thin films and Ag_2S tips. The electron dispersive X-ray spectrometer EDS) was used to characterize elemental composition and elemental mapping. ImageJ (ver. 1.51j8, Wayne Rasband, National Institutes of Health, USA) was used to calculate the Ag NFs density and length.

3.2.5.2. Electrochemical reduction

Potentiostat is an optional method which was chose to construct the Ag filaments on Ag_2S thin film. The electrochemical cell can be set up with 2 electrodes as shown in Figure 3.2. The copper was used as working electrode (WE) and Ag_2S thin film was used as counter electrode (CE). A linear sweep voltammetry potentiostat was used to apply voltage. The voltage was applied in 0.5 V. The scan rate was used in 0.01 V/s. After the reaction, the thin film was rinse with DI water and blew with N_2 gas. The thin film was characterized by FE-SEM for morphology study with 20 kV of accelerated voltage. The chemical composition of thin film was measured by XRD, UV-Vis spectrometry and EDS mapping. The UV-Vis was taken in the range of 300-1000 nm.

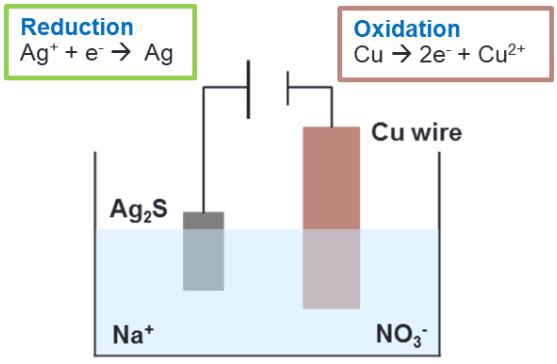

Figure 3.2. Schematic representative of the 2 electrode setup

3.3 Application test

3.3.1. SERS Measurement

The SERS performance using Ag NFs on Ag_2S thin films (Ag/Ag_2S) as a SERS substrate fabricated via electron irradiation in SEM was observed. Methylene blue (MB), Raman active molecules, was employed for testing SERS activity. The 10^{-3} M (in aqueous) MB solution was dropped on the Ag NFs/Ag_2S substrates and dried for 15 min in the ambient air. The microscopic confocal Raman spectroscope using a laser beam with an excitation wavelength of 532 nm, 600/600 grating and charge-couple device (CCD) with a resolution of 4 cm^{-1} was employed to record the SERS spectra. The SERS spectra were acquired with exposure time of 10 s and 3-times accumulations. The area of Raman imaging was 100 μm^2. The exposure time of scan speed and resolution of imaging were 0.3 s per pixel and 32x32 pixel, respectively. The limit of detection (LOD) of Ag NFs SERS substrate also was measured at 10^{-3}, 10^{-4}, 10^{-6}, 10^{-8}, $10^{-9}$and 10^{-10} mM of MB.

3.3.2. TERS performance measurement

The Ag NFs on Ag_2S tip (Ag NFs/Ag_2S) were used for TERS studies. The 10^{-3} M MB solution was dropped on the Ag NFs/Ag_2S tip and dried for 15 min in the ambient air. The microscopic confocal Raman spectroscope using a laser beam with an excitation wavelength of 532 nm and charge-couple device (CCD) with a resolution of 4 cm^{-1} was employed to record the SERS spectra. The Raman spectra were acquired with exposure time of 10 s and 3-times accumulations. A tapping mode AFM was used for an in-depth understanding of the surface by using Ag NFs/Ag_2S tip.

CHAPTER IV
RESULTS AND DISCUSSION

4.1. Fabrication of Ag thin films

Ag thin films with the thickness of 100 nm were prepared on Si (100) substrates (1x1 cm^2) by RF magnetron sputtering technique as shown in Figure 4.1. The Ag thin film looked to have luster compared to Si wafer.

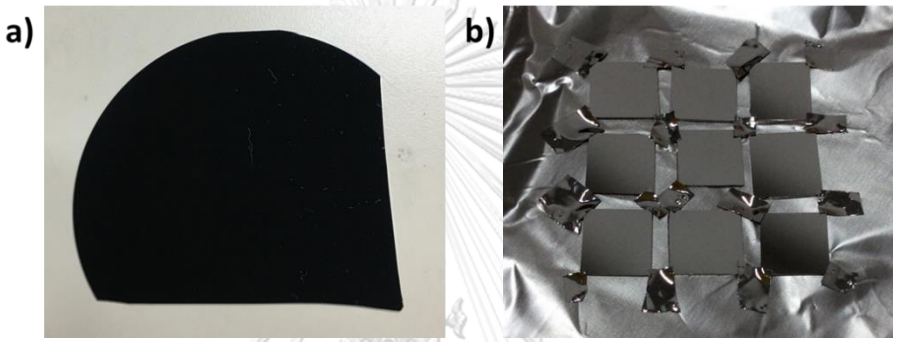

Figure 4.1 a) Si (100) wafer and b) The 100 nm thick Ag Thin film prepared by RF magnetron sputtering technique

The morphology of Ag thin film was studied by AFM and SEM. Figure 4.2a shows the AFM image of the 100 nm thick Ag thin films with average roughness (R_a) and root mean square (RMS) roughness of 1.6 nm and 2.0 nm, respectively. Figure 4.2b shows the top view SEM image of the 100 nm thick Ag thin films with the magnification of 30,000.

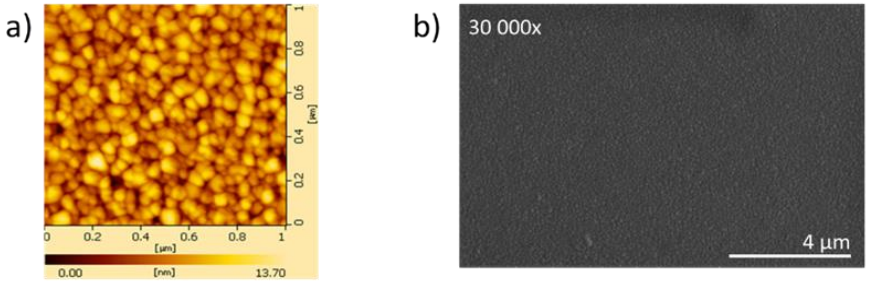

Figure 4.2 a) AFM image with the area of 1x1 μm^2, b) top view SEM image of Ag thin films prepared by RF magnetron sputtering technique.

Moreover, EDS mapping was used to investigate the elemental analysis of a cross section of 100 thick Ag thin film as shown in Figure 4.3. The sequence of Ag thin film from the bottom to top layers is Si (substrate), Ti (adhesive layer), and Ag, respectively. It should be noted that oxygen (O) mapping could also be observed in thin film. This could be titanium dioxide (TiO_2) generated during Ti film sputtering due to O_2 gas remained in the sputtering chamber and oxidized during subsequent experiments.

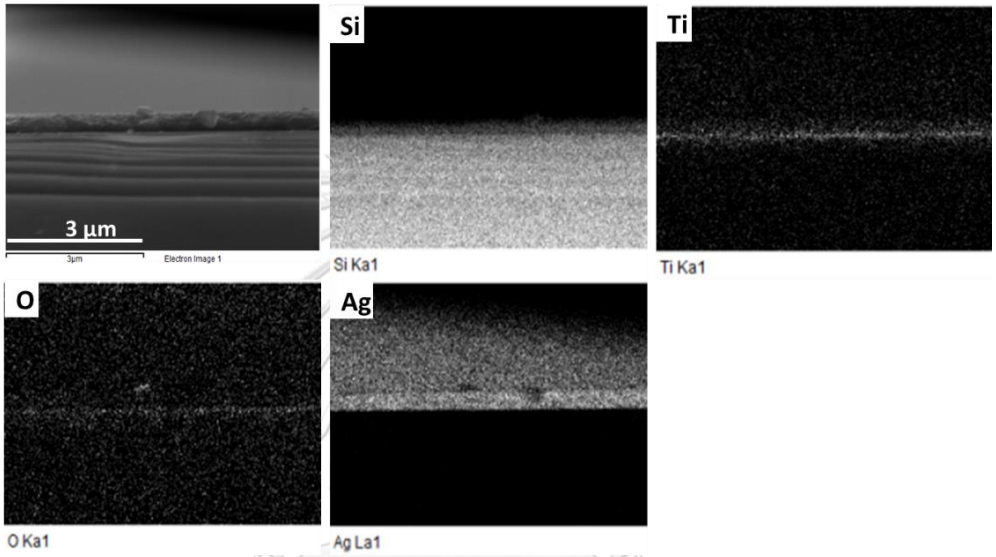

Figure 4.3 Ag on the cross-section of the 100 nm thick Ag thin film and elemental distribution of Si, Ti, O , and Ag.

Then, the 100 nm thick Ag thin film was characterized by XRD spectrometry as shown in Figure 4.4. The XRD spectra show that the Ag thin film were composed of Ag (111) and Ag (200) peaks compared to the Si substrate which Si (100) could be observed. Since Ag (111) and Ag (200) are the major diffraction pattern of face-centred-cubic (FCC) of Ag thin film structure according to the Joint Committee in Powder Diffraction Standards (JCPDS) file No. 04-0783. The high intensity ratio of Ag (111)/Ag (200) peak was obtained at 4.61. This Ag thin film with high amount of Ag (111) was suitable for the next step of sulfurization with Na_2S due to the preferential plane of Ag (111) with Sulphur ions.

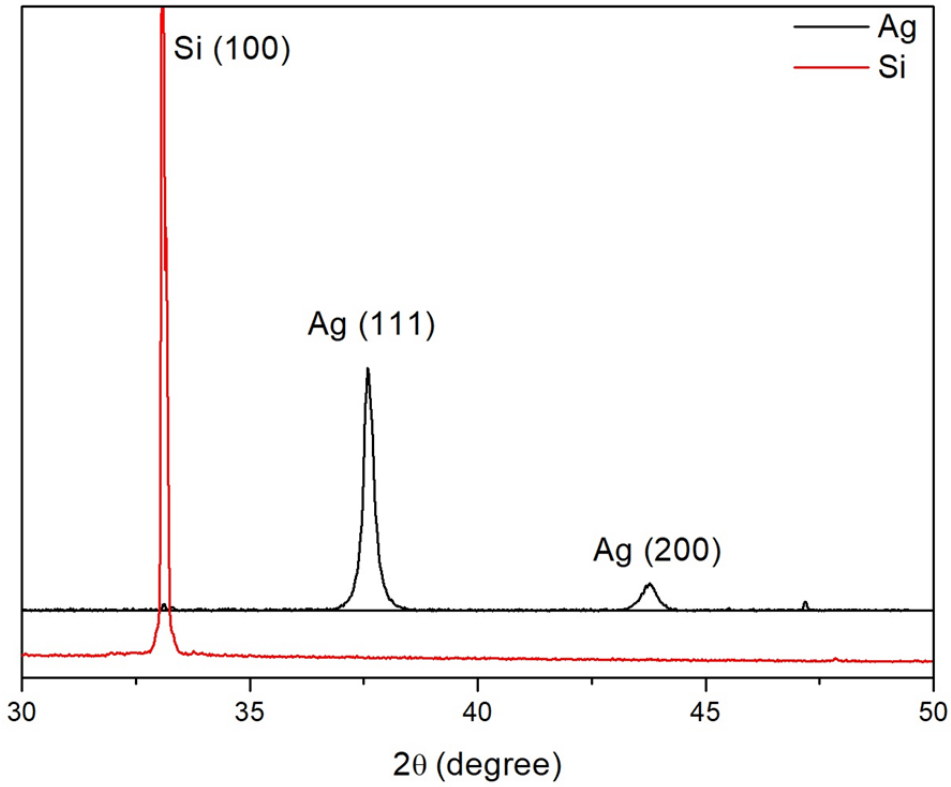

Figure 4.4 The XRD spectra of Ag thin film and Si substrate

4.2. Fabrication of Ag_2S thin films

After the 100 nm thick Ag thin films were grown on Si (100) substrates, the preliminary study of Ag_2S thin films fabrication was carried out by wet chemical process, The Ag thin films were dipped into 0.1 M Na_2S for 6 h. The temperature was varied at room temperature (RT), 50, 90 and 120 °c. The higher temperature used, the higher kinetic energy of molecules obtained leading to the high sulfurization rate. At 50, 90, 120 °c, the delamination of Ag thin films was observed (data not shown). This can be attributed to complete sulfurization of Ag thin film with high Na_2S concentration and high basic solution at high temperature. The less amount of Ag was left and Ag_2S thin film could not be attached onto Ti layer. After that the effect of Na_2S concentration was studied. The Na_2S concentration was reduced to 20 mM. The result shows that the color of Ag thin film prepared at room temperature was changed from metallic to dark brown as shown in Figure 4.5. This indicates that the chemical reaction was occurred.

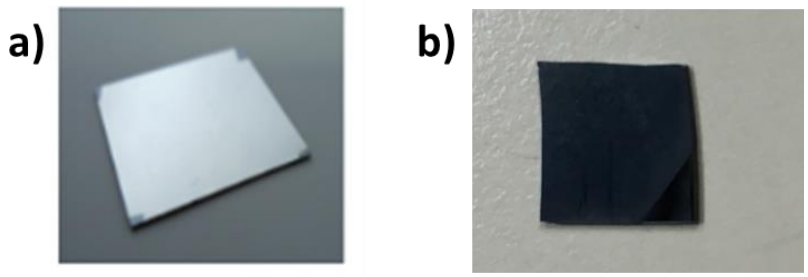

Figure 4.5 a) Ag thin film and b) Ag_2S thin film prepared by dipping Ag thin film into 20 mM Na_2S solution for 6 h dipping time.

The chemical composition of Ag_2S thin film was characterized by XRD and Raman spectroscopy as shown in Figure 4.6. Figure 4.6a demonstrates the Raman spectrum of Ag_2S thin film that consists of Ag-S stretching peak at Raman shift of 243 cm^{-1}. The X-ray profile analysis of Ag_2S thin films (Figure 4.6b) shows Ag (111) and Ag (200) peaks. The mixture of crystal structures of **α**-Ag_2S, acanthite structure, and **β**-Ag_2S, argentite structure, was observed in Ag_2S thin films. The obtained amount of **β**-Ag_2S was still low with the Na_2S concentration of 20 mM so the variation of Na_2S concentration was studied.

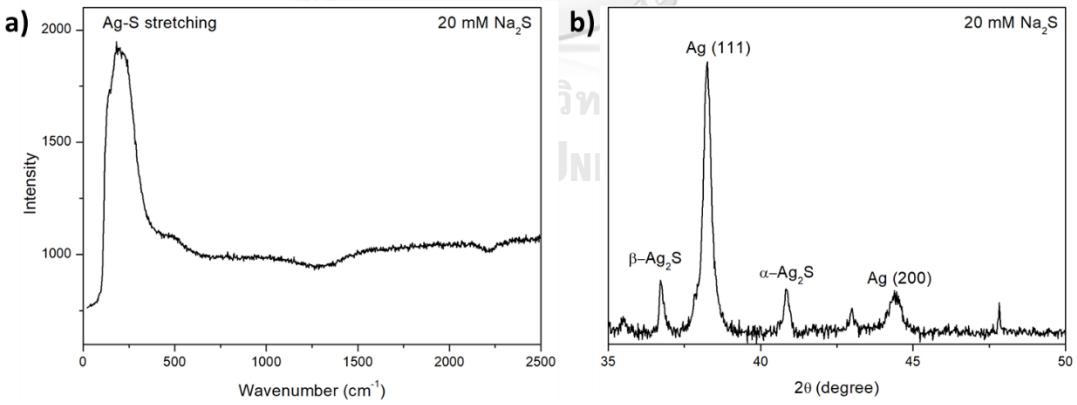

Figure 4.6 a) Raman spectrum and b) XRD spectrum of Ag_2S thin film prepared by dipping Ag thin film into 20 mM Na_2S solution for 6 h.

4.2.1. Effect of high Na_2S concentration and dipping time on β-Ag_2S synthesis

The concentration of Na_2S was studied at 10, 20, 30, 50 and 80 mM and the dipping time was varied at 3, 6, 12 and 24 hours. The chemical composition was studied by using UV-vis spectroscopy and XRD. The XRD spectra of Ag_2S thin films prepared with different dipping time at 20 mM Na_2S were shown in Figure 4.7.

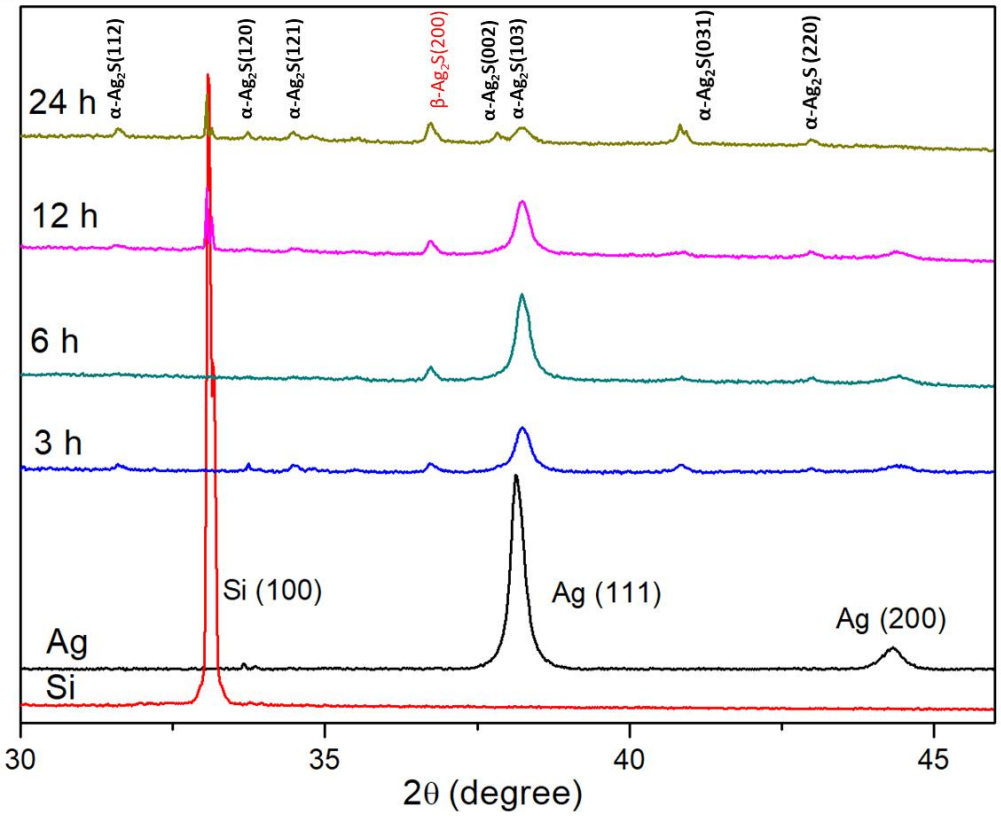

Figure 4.7 XRD spectra of Si, Ag thin film and Ag_2S thin films prepared by dipping Ag thin films into 20 mM Na_2S solution at different dipping time of 3, 6, 12 and 24 h.

The XRD results show the mixture of β-Ag_2S and α-Ag_2S phases for all dipping time. The intensity of Ag (111) and Ag (200) peaks decreased when the dipping time increased. This indicates that both Ag (111) and Ag (200) reacted with Na_2S to form both β-Ag_2S and α-Ag_2S phases. The XRD intensity of β-Ag_2S and Ag (111) was then investigated since Ag (111) is the preferential plane for reaction. The relationship between intensity ratio of β-Ag_2S to Ag (111) obtained from XRD spectra in Figure 4.7

and dipping time at different Na_2S concentrations was shown in Figure 4.8. It was found that the amount of β-Ag_2S was significantly increased at the lower Na_2S concentration between 10 and 30 mM. There was a slight increase of the amount of β-Ag_2S at 50 mM Na_2S while there was no change of the amount of β-Ag_2S at the highest concentration of 80 mM. This is due to the higher Na_2S concentration used, the higher pH obtained. This can lead to the corrosion of Ag_2S thin film surface.

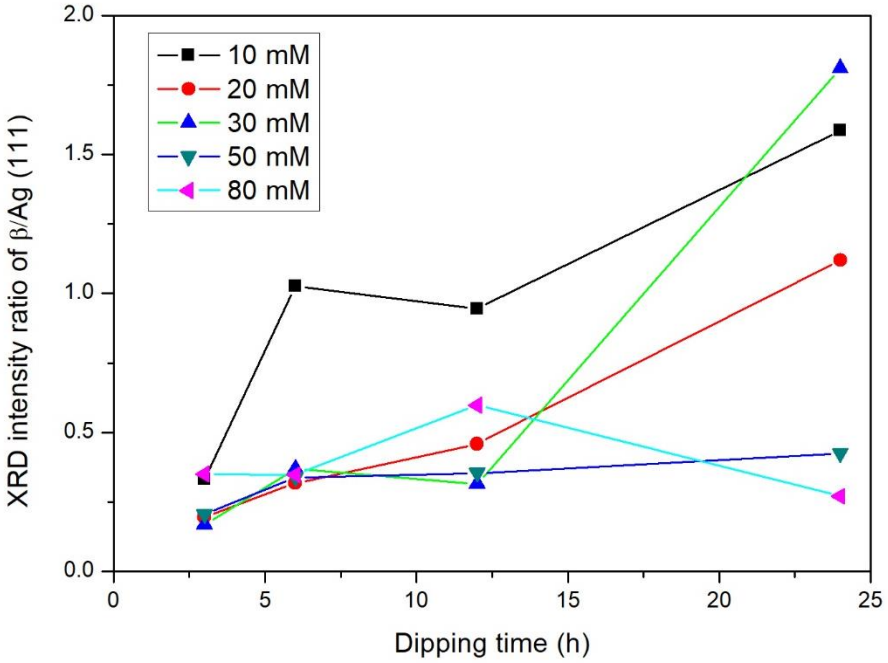

Figure 4. 8 The Relationship between dipping time of 3, 6, 12 and 24 h and the XRD intensity ratio of β-Ag_2S to Ag (111) obtained from Figure 4.7 at different Na_2S concentrations.

To deeply understand this phenomena, AFM was employed to investigate the Ag_2S surface morphology as shown in Figure 4.9. AFM images of all Ag_2S thin films reveal that the roughness of all Ag_2S thin film surfaces was higher than the roughness of Ag thin film. This indicates that the sulfurization was occurred. The higher Na_2S concentration leads to the higher pH and the delamination of the surface occurred at 80 mM. This result was well correlated to the XRD result with the decrease of the amount of β-Ag_2S at 80 mM Na_2S (see Figure 4.8).

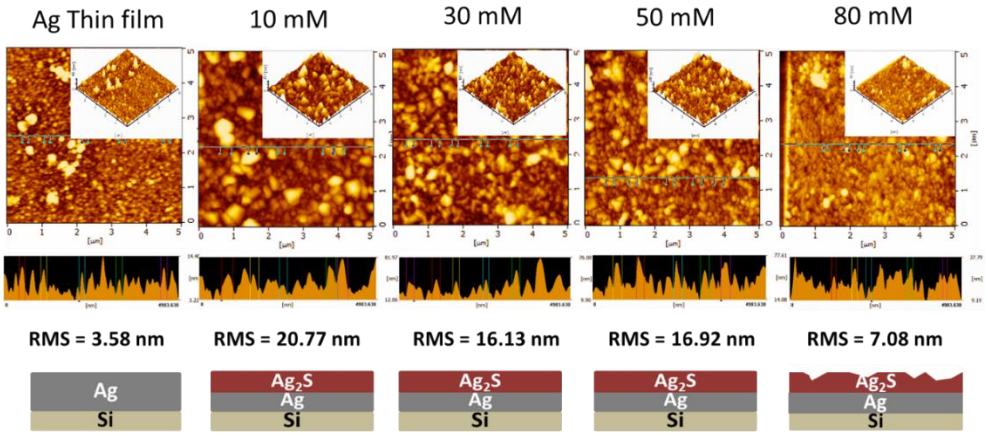

Figure 4.9 AFM images of Ag and Ag_2S thin films prepared from different Na_2S concentrations of 10, 30, 50 and 80 mM for 6h dipping time.

The preliminary study of Ag NFs was studied by using e^- irradiation by FE-SEM with 5 kV of accelerated voltage and 10 min of irradiation time on Ag_2S thin film prepared from 20 mM Na_2S for 6 h of dipping time (Figure 4.10). The result shows that Ag NFs were fabricated on the Ag_2S surface. The low density of Ag NFs was observed due to the small amount of **β**-Ag_2S (Figure 4.8). So the effect of Na_2S concentration at lower concentration was studied.

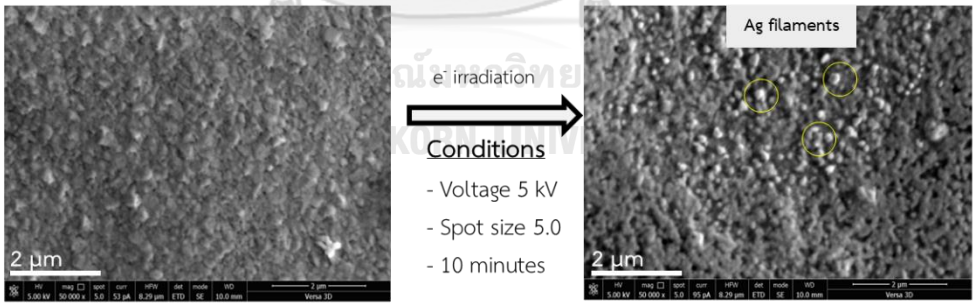

Figure 4.10 The method for e- irradiation with 5 kV of accelerated voltage and 10 min of irradiation time on Ag_2S prepared by 20 mM of Na_2S for 6h. of dipping time

4.2.2. Effect of low Na_2S concentration on **β**-Ag_2S synthesis

Due to the less Ag NFs fabrication, the low Na_2S concentration was studied at 2 mM of Na_2S and 6 h. of dipping time.

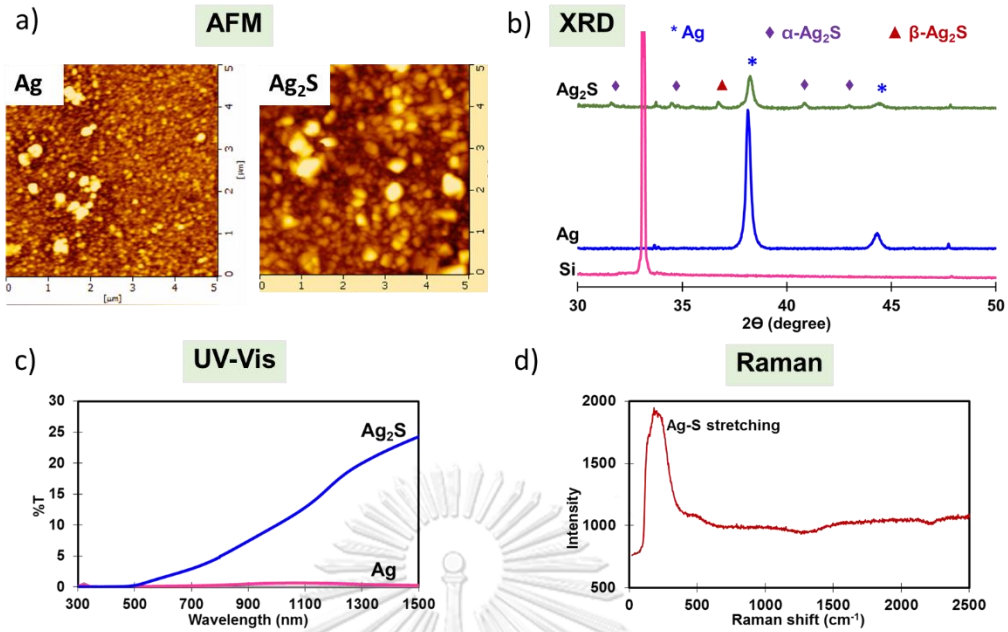

Figure 4.11 The characterization of Ag and Ag_2S thin films prepared from 2 mM Na_2S solution for 6 h. a) AFM images of Ag and Ag_2S thin films, b) XRD patterns of Ag, Ag_2S and Si with 2Θ = 30-50°, c) UV-Vis spectra of Ag_2S and Ag thin films and d) Raman spectrum of Ag_2S thin films

Figure 4.11 a). RMS roughness of Ag_2S thin film with 16.9 nm is higher than that of Ag thin film with 3.6 nm. This indicates that the morphology of Ag thin film was changed after the sulfurization reaction. The X-ray profile of Ag_2S thin films compared to those of Ag and Si thin films (Figure 4.11b) reveals that both of Ag and Ag_2S thin films include Ag (111) and Ag (200) peaks. Mixture-phase crystal structures of α-Ag_2S, acanthite structure, and β-Ag_2S, argentite structure, were observed in Ag_2S thin films. The optical transmittance of Ag and Ag_2S was studied by using UV-Vis spectrophotometer. The results are shown in Figure 4.11c) indicating that transmittance (%T) of Ag_2S was higher than that of Ag thin film. Figure 4.11d) demonstrates the Raman spectrum of Ag_2S thin film that consists of Ag-S stretching peak at Raman shift of 243 cm^{-1}.

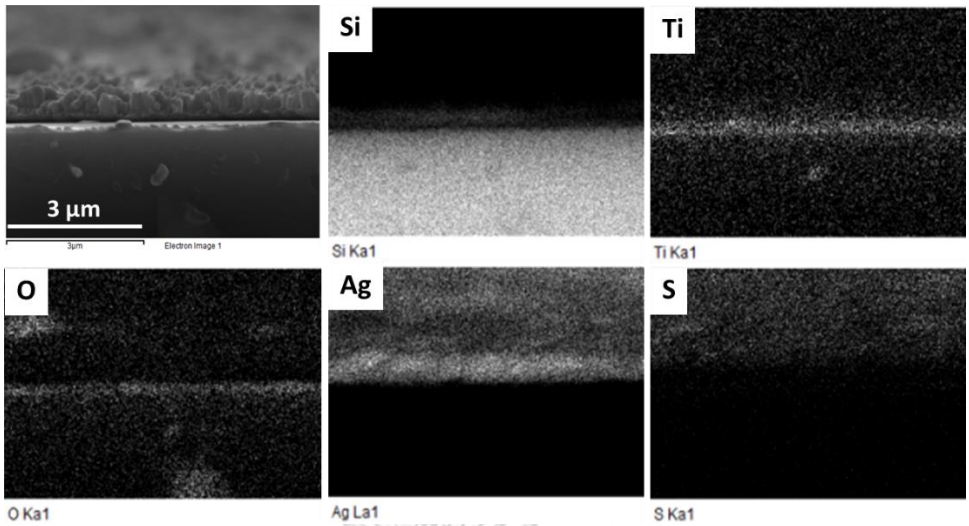

Figure 4.12 SEM image of the cross-section of Ag_2S thin film prepared by 2 mM Na_2S solution and 6 h dipping time and elemental distributions of Si, Ti, O, Ag, and S

The elemental analysis of Ag_2S thin film was studied by using EDS mapping on the cross-section SEM image of Ag_2S thin film prepared by 2 mM Na_2S solution and 6 h dipping time. Figure 4.12 shows that the Ag_2S thin film from the bottom to top layers is composed of Si (substrate), Ti (adhesive layer), Ag (Ag film, Ag_2S thin film and filaments), and S (Ag_2S thin film), respectively. The oxygen (O) mapping could also be observed due to titanium dioxide (TiO_2) generated during Ti film sputtering.

Moreover, the sequence of elemental layers of Ag_2S thin film was also characterized by XRF as shown in appendix (Figure A.2). From the results, Si, S, Ag and Ti (adhesive layer) were found on the surface that agreed well with EDS results in Figure 4.12. These elements were uniformly distributed throughout the surface which indicates that Ag_2S thin film was fully synthesized on the surface by Na_2S and Ag thin film. Various concentrations of Na_2S aqueous solutions were studied for the synthesis of **β**-Ag_2S. The Na_2S concentrations were studied at 0.5, 2, 5, 10, and 20 mM and the dipping time was varied at 3, 6, 12 and 24 hours. The relationship between intensity ratio of **β**-Ag_2S and **α**-Ag_2S (I_β/I_α) from XRD spectra and Na_2S concentrations of 0.5, 2, 5, 10 and 20 mM and dipping time of 3, 6, 12 and 24 h are shown in Figure 4.13 a) and b), respectively. At low Na_2S concentration (0.5 – 2 mM), the highest I_β/I_α was found at

6 h of dipping time due to the low sulfidation rate. On the other hand, the high Na_2S concentration (10 – 20 mM), the highest $I\beta/I\alpha$ was found at 3 h of dipping time due to the high sulfurization rate. The highest $I\beta/I\alpha$ was found at 0.5 mM Na_2S and dipping time of 6 h. It can be seen that when the concentration of Na_2S increased from 0.5 mM to 20 mM at 6 h, the $I\beta/I\alpha$ significantly decreased from 10 to 1 as shown in Figure 4.13b). This can be attributed to the higher concentration of Na_2S, the faster the reaction rate of sulfidation leading to the lower rearrangement of Ag_2S unit cell. The sulphur ions were preferentially deposited on Ag (111) surface. Since the sulphur deposition rate is slower at lower concentration of Na_2S, Ag_2S was gradually rearranged to form β-Ag_2S BCC unit cell which is denser unit cell than α-Ag_2S monoclinic unit cell [51].

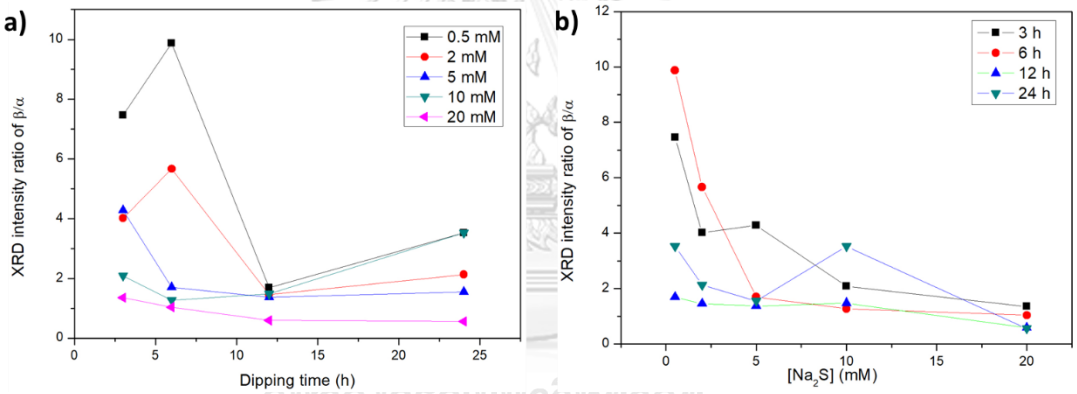

Figure 4.13 Relationship between the XRD intensity ratio of β-Ag_2S to α-Ag_2S and a) dipping time of 3, 6, 12 and 24 h and b) Na_2S concentration of 0.5, 2, 10 and 20 mM

The Relationship of Na_2S concentration and dipping time to %T which can refer to the amount of Ag_2S were also studied as shown in Figure 4.14. Na_2S concentration increased, %T was increased. Dipping time (3, 6, 12 h.) increased, was increased and %T was decrease at 24 h. of dipping time. Figure 4.14a) shows that the Ag_2S fabrication at lower Na_2S concentration (0.1-5 mM) took a longer reaction time than that at higher Na_2S concentration (10-80 mM) due to the high initial reaction rate of the high concentration. However, it can be observed that there was the saturation of the reaction of all Na_2S concentrations after 12 h. Consequently, it can be concluded that

both of Na_2S concentration and dipping time have a strong effect on the amount of Ag_2S. The highest **β**-Ag_2S was obtained at the 0.5 mM Na_2S concentrationand 6 h dipping time.

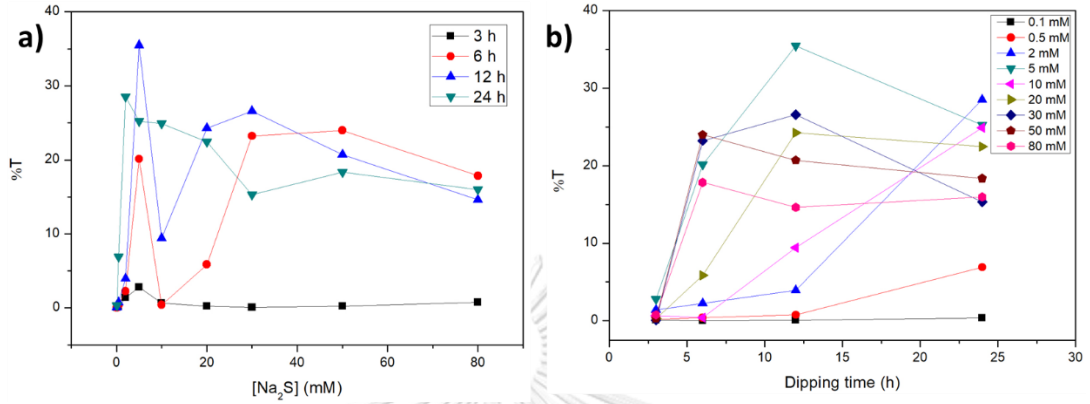

Figure 4.14 Relationship between the %T and a) Na_2S concentration of 0.1, 0.5, 2, 5, 10, 20, 30, 50 and 80 mM and b) dipping time of 3, 6, 12 and 24 h of each Ag_2S thin film separately prepared from the 100 nm of Ag thin films.

4.2.3. Effect of pH Na_2S solution on **β**-Ag_2S synthesis

The effect of pH on **β**-Ag_2S formation was studied because the different Na_2S concentrations cause the different pH of Na_2S solutions. It was synthesized in both acidic and basic solution by adding HNO_3 and NaOH, respectively Na_2S solutions. When the Na_2S concentration was increased, pH increased as shown in Figure 4.15a) because the hydrolysis of Na_2S gives the OH^- ions in the solution. The hydrolysis reaction mechanism is proposed according to the following reactions:

$$Na_2S + H_2O \rightleftharpoons NaHS + Na^+ + OH^- \quad (1)$$

$$NaHS + H_2O \rightleftharpoons H_2S + Na^+ + OH^- \quad (2)$$

In acidic solution, when HNO_3 was added H^+ ion reacted with OH^- ion to form H_2O. Then the equilibrium is shifted towards the products, concentration of S^{2-} ion for sulfurization decreased. This leads to the low amount of **β**-Ag_2S obtained. The higher concentration of Na_2S gives the higher OH^- ions in the solution. Figure 4.15 b) shows that the highest **β**-Ag_2S amount was obtained at pH 8.45. **β**-Ag_2S decreased when pH

increased due to the corrosion of Ag_2S surface. So the optimum solution of pH is about 8.45 which is equal to 0.5 mM Na_2S.

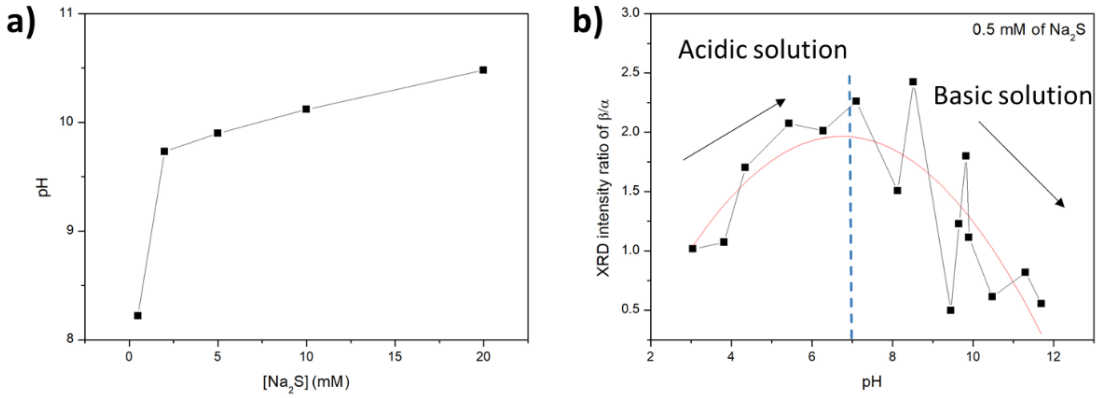

Figure 4.15 a) The relationship between the pH and Na_2S concentration and b) the XRD intensity ratio of **β**-Ag_2S to **α**-Ag_2S with 0.5 mM Na_2S for 6h of dipping time. The acidic and basic solution were prepared by adding HNO_3 and NaOH into 0.5 mM Na_2S solution, respectively

4.3. Fabrication of Ag NFs

4.3.1. Effect of irradiation time on Ag NFs fabrication

Ag NFs fabrication was studied by using e^- irradiation on Ag_2S thin films with the acceleration voltage of 20 kV and beam current of 3.8 nA with different irradiation time of 1, 5 and 10 min as shown in Figure 4.16. Figure 4.16 a) shows that Ag filaments were rapidly formed by the reduction of Ag_2S to Ag after 1 min. After that, Ag filaments were vertically grown significantly after irradiation for 5 minutes (see Figure 4.16 b)) and gradually grown in the vertical direction after 10 min irradiation (see Figure 4.16c)).

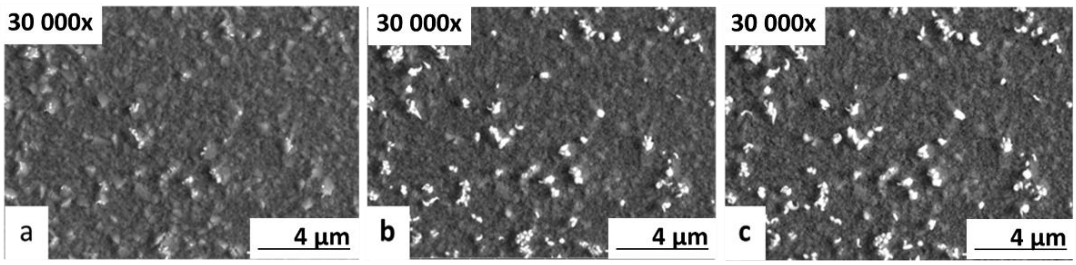

Figure 4.16 Ag filaments grown by electron beam irradiation on Ag_2S film prepared by 2 mM Na_2S at 6h of dipping time with 20 kV acceleration voltage and 3.8 nA current with different irradiation time of (a) 1 min (b) 5 min and (c) 10 min.

The SEM image at 50000x magnification (see Figure 4.17 a)) shows that the Ag filaments were in the nanoscale size. SEM image at 25000x magnification (see Figure 4.17 b)) shows the larger area between the focus (electron) area and the area of Ag_2S thin film as shown in Figure 4.17 b). This reveals that the Ag NFs fabrication was only formed on Ag_2S surface after irradiation with e^- beam. The mechanism of Ag NFs formation can be conventionally divided into three steps. For the first step, the e^- beam focused on Ag_2S surface results in the heat generation on the surface leading to the residue stress of the surface [52]. This can lead to the formation of **β**-Ag_2S nuclei taking place on the Ag_2S surface. Moreover, the **α**-Ag_2S can be transformed to **β**-Ag_2S by heat generation. The second step is related to the diffusion of the Ag^+ ions inside the lattice of **β**-Ag_2S to the surface of **β**-Ag_2S. These Ag^+ ions can accept the e^- from e^- irradiation. The Ag NFs were then formed by reduction of Ag^+ ions to Ag. Since the S ions form a rigid bcc lattice with Ag cations which are randomly occupying 1/3 of 12 d sites in the lattice (Wyckoff symbols) [53]. The 12 d position has a hexagonal symmetry which has the minimal lattice mismatch with Ag (111). In the last step, the Ag^+ ions from the oxidation of Ag thin film can act as Ag backup for increasing length of Ag NFs.

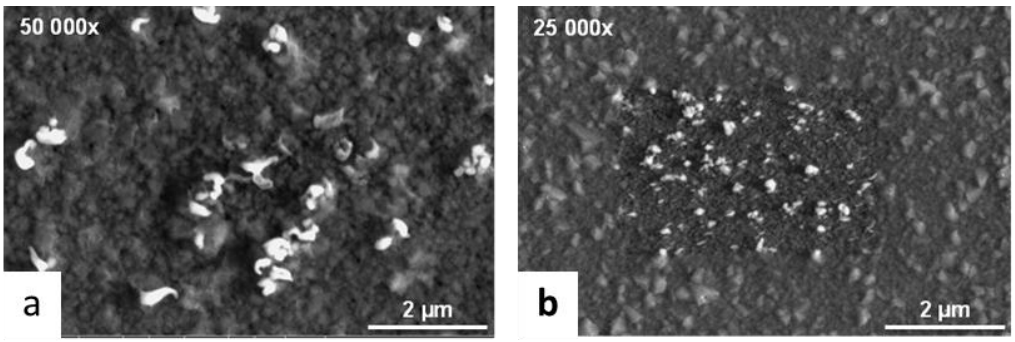

Figure 4.17 The Ag filaments with (a) 50000x (b) 25000x magnification

To deeply understanding the effect of heat generation of e^- beam, the electrochemical process was studied. A linear sweep potentiostat is an optional method which was chosen to construct the Ag filaments on Ag_2S thin film. The Ag_2S thin film was used as working electrode (S/WE) and copper wire was used as counter electrode (RE/CE). We applied the potential in the range of 0-5 V and the scan rate of 0.01 V/s as shown in Figure 4.18.

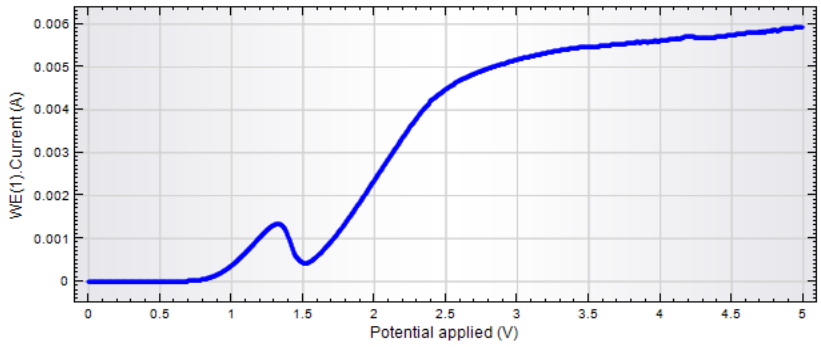

Figure 4.18 The relationship between applied potential and WE (Ag_2S) current of cell with copper as CE.

After the electrochemical reaction, the Ag_2S thin film was turned to silver colour. This is because the Ag_2S thin film (Ag^+) was reduced to Ag. The blue thin film colour was appeared on the surface of copper electrode indicating that the oxidation reaction was occurred. The blue film was Cu^{2+} as shown in Figure 4.19.

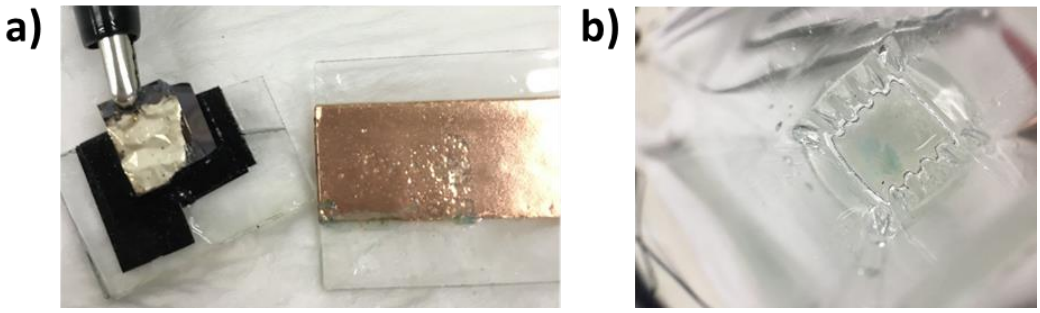

Figure 4.19 a) The Ag_2S thin film and copper electrode after the reaction and b) a blue residue film in the electrolyte solution ($NaNO_3$)

To investigate the Ag thin film prepared from electrochemical reaction (Ag_{elec}), the Ag_2S thin film was characterized by EDS as shown in Figure 4.20. The EDS spectrum shows that there was no sulphur on the thin film (see Figure 4.20 b) and c)) which indicates that the reduction of Ag_2S to Ag was completely generated. However, the Na^+ ions of electrolyte were also being growth on the Ag_{elec} thin film (Figure A.1)

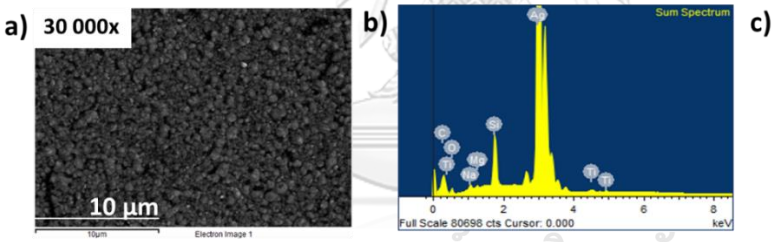

Element	Weight%	Atomic%
C K	1.98	11.54
O K	3.97	17.35
Na K	0.63	1.91
Mg K	0.22	0.62
Si K	4.20	10.46
Ti K	0.45	0.66
Ag L	88.55	57.45
Totals	100.00	

Figure 4.20 a) SEM image of the Ag_{elec} thin film, b) the elemental distribution of EDS spectrum and c) the percentage of elements.

Moreover, UV-vis spectroscopy was also used to characterize the Ag_{elec} fabrication. A glass slide was used as a substrate for transmission measurements. After the electrochemical reaction, the Ag_2S thin film was change to Ag thin film (Figure 4.21b)). The UV transmittance spectra of Ag_2S and Ag_{elec} thin film taken in the range of 300-1000 nm is shown in Figure 4.21 c). The Ag_2S thin film shows a high transmittance in the near-infrared region at the wavelength of 1240 nm. While Ag_{elec} film demonstrates 0% transmittance from visible to near-infrared region. This result indicates that the Ag_2S was converted to Ag film.

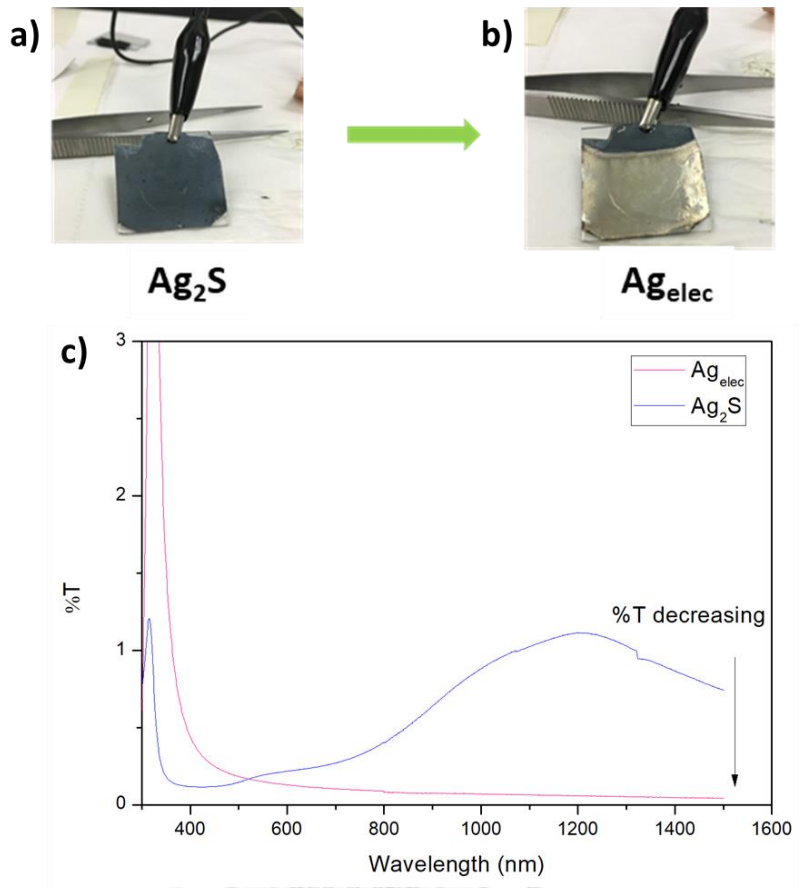

Figure 4.21 a) Ag_2S thin film and b) Ag_{elec} thin film after the electrochemical reaction and c) UV-vis spectra of Ag_2S and Ag_{elec} thin films.

To understand the above result, XRD was used to study the electrochemical reaction of Ag_2S film. Figure 4.22 shows the XRD spectra of Ag_{elec} thin film compared to Ag thin film prepared from sputtering technique (Ag_{sputt}). From the results, the electrochemical method can convert both **α**-Ag_2S and **β**-Ag_2S film to Ag thin film which is composed of Ag (111) and Ag (200) planes. The Ag (111)/Ag (200) ratio of Ag_{elec} and Ag_{sputt} thin films was calculated as 4.61 and 5.60, respectively. So the higher amount of Ag (111) plane was obtained from sputtering technique compared to the electrochemical reaction. This can be concluded that the potentiostatic method was not suitable process for Ag NFs fabrication due to the obtaining of Ag thin film.

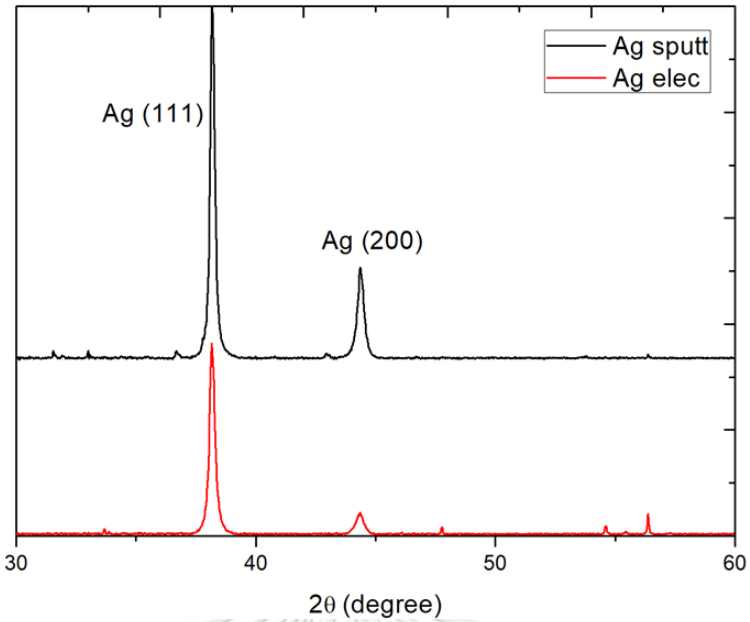

Figure 4.22 The XRD spectra of Ag_{sputt} film and Ag_{elec} film

4.3.2. Effect of β-Ag_2S on Ag NFs fabrication

After the optimum condition to obtain the highest amount of β-Ag_2S thin film was achieved from the previous section, the effect of β-Ag_2S amount on Ag NFs formation was studied. The irradiation condition used was 20 kV of accelerated voltage and 10 min of irradiation time. When the concentration of Na_2S increased from 0.5 to 20 mM, the density of Ag NFs decreased from 5.93 x 10^9 NF/cm^2 to 1.09 x 10^8 NF/cm^2 as shown in Figure 4.23. This result was in good agreement with the amount of β-Ag_2S as shown in Figure 4.13. and agree well with the study of Tanaka *et al.* According to the study of the electron irradiation, β-Ag_2S argentite which has a superionic conductivity can be transformed to Ag via electron irradiation. Ag^+ ions in β-Ag_2S can be diffused faster along the line and surface defects than that in α-Ag_2S. This is because Ag^+ ions in β-Ag_2S are at the center of unit cell while Ag^+ ion in α-Ag_2S is in the lattice. The linear diffusion is faster than the lattice diffusion, they are also termed as high diffusivity or easy diffusion paths [54]. The diffused Ag^+ ion was reduced on the surface of the thin film to form Ag NFs. Our results confirm that β-Ag_2S has a strong effect on Ag NFs growth.

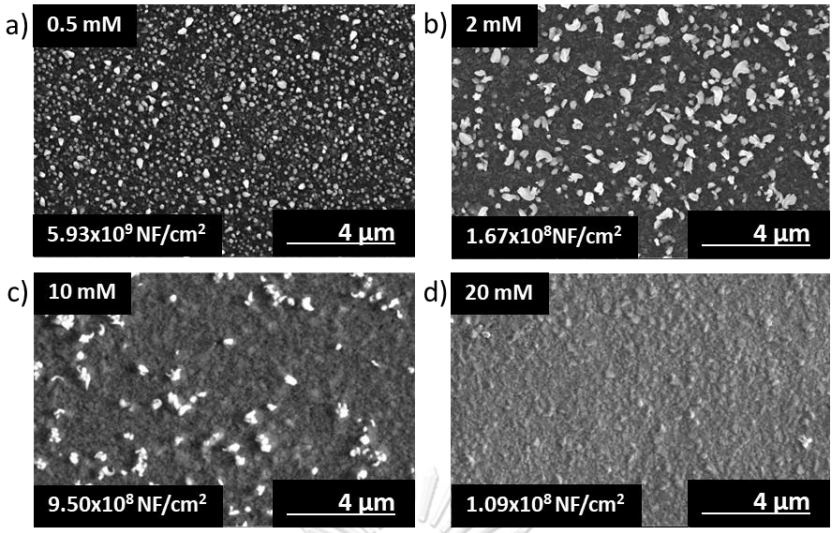

Figure 4.23 SEM images of Ag NFs after irradiation with 20 kV for 10 min. The scanning area is 13.8 x 13.8 μm^2. (The samples were prepared by dipping into different concentrations of 0.5, 2, 10 and 20 mM of Na_2S for 6 h)

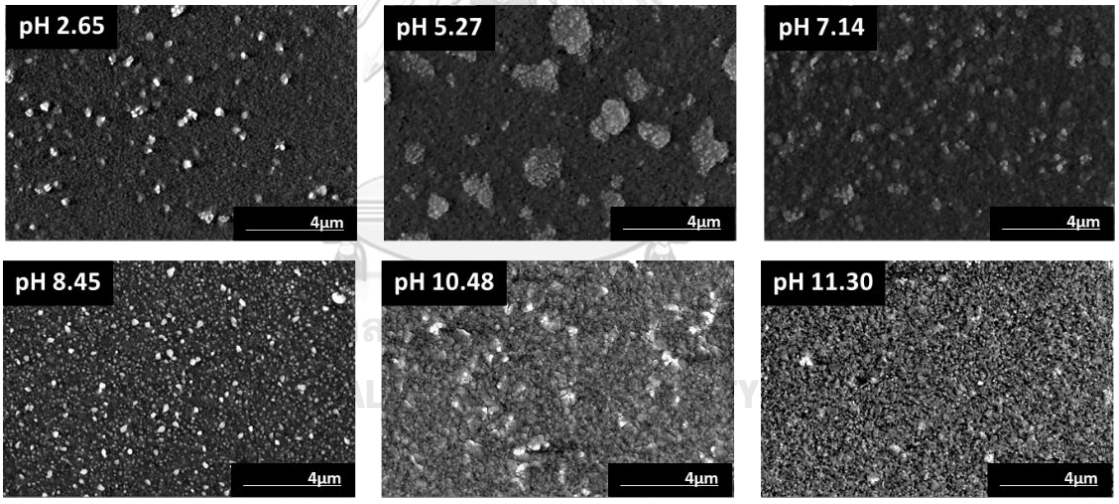

Figure 4.24 SEM images of Ag NFs after irradiation with 20 kV for 10 min. The scanning area is 13.8 x 13.8 μm^2. The samples were dipped into 0.5 mM of Na_2S for 6 h. The acidic and basic solution were prepared by adding HNO_3 and NaOH into Na_2S solution, respectively.

From Figure 4.24, the highest density of 1.09 x 10^9 NFs/cm^2 was found at pH 8.45. This result was well correlated to the XRD study in Figure 4.15 b) that the highest amount of β-Ag_2S was obtained at pH 8.45.

4.3.3. Effect of accelerated voltage on Ag NFs fabrication

From section 4.3.1, the optimum condition of irradiation time for Ag NFs fabrication was found at 10 min, Then, the effect of irradiation parameters namely accelerated voltage (kV) on the fabrication of Ag NFs was studied as shown in Figure 4.25. It can be observed that the density of Ag NFs fabricated by using 20 kV for 10 min was higher than those fabricated by 10 kV and 5 kV for 10 min. The higher voltage used, the faster and higher kinetic energy electrons generated. These fast and high kinetic energy electrons can then react and diffuse on the Ag_2S surface to form Ag NFs. Moreover, the longer irradiation time was used to irradiate on Ag_2S surface, the higher kinetic energy electrons were generated and could react with β-Ag_2S thin film. Consequently, the optimum condition of electron irradiation for Ag NFs fabrication was 20 kV for 10 min for accelerated voltage and irradiation time, respectively.

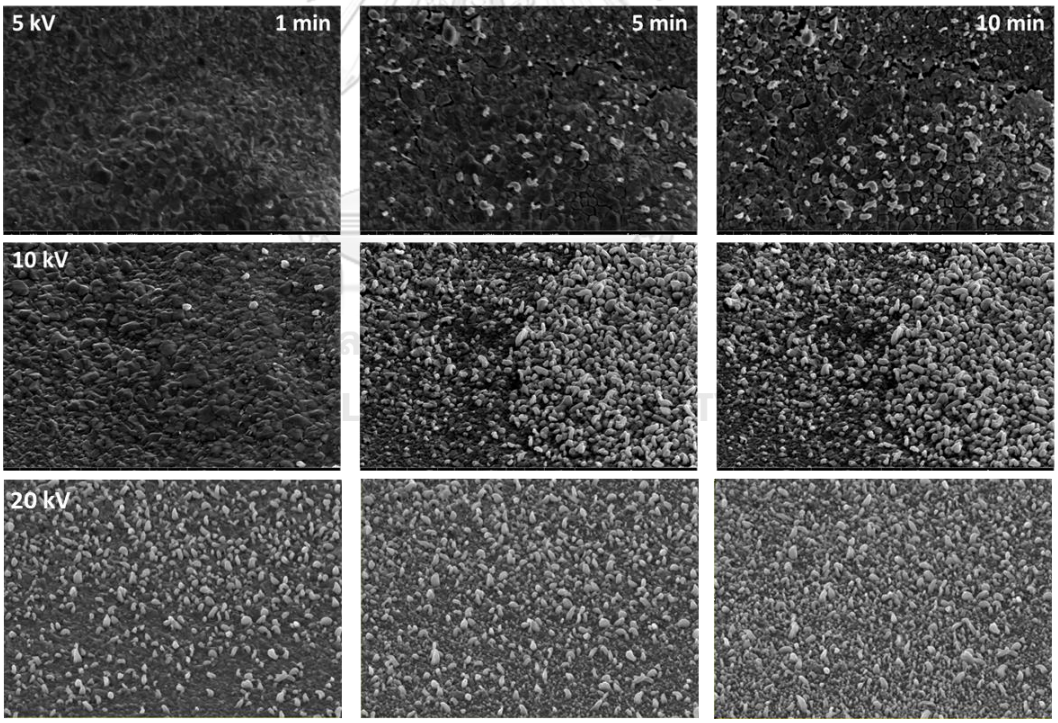

Figure 4.25 SEM images of Ag NFs on Si substrates prepared by dipping Ag thin film into 0.5 mM Na_2S solution for 6 h and irradiated by different accelerated voltages at 5, 10, 20 kV for 1, 5 and 10 min.

The effect of accelerated voltage and irradiation time on the fabrication of Ag NFs can be plotted as a graph between the density of Ag NFs and irradiation time which is presented in Figure 4.26 a). Moreover, the length of Ag NFs as a function of irradiation time is shown on Figure 4.26 b). The results show that the highest length of Ag NFs was 0.46 ± 0.04 μm obtained at 20 kV for 10 min.

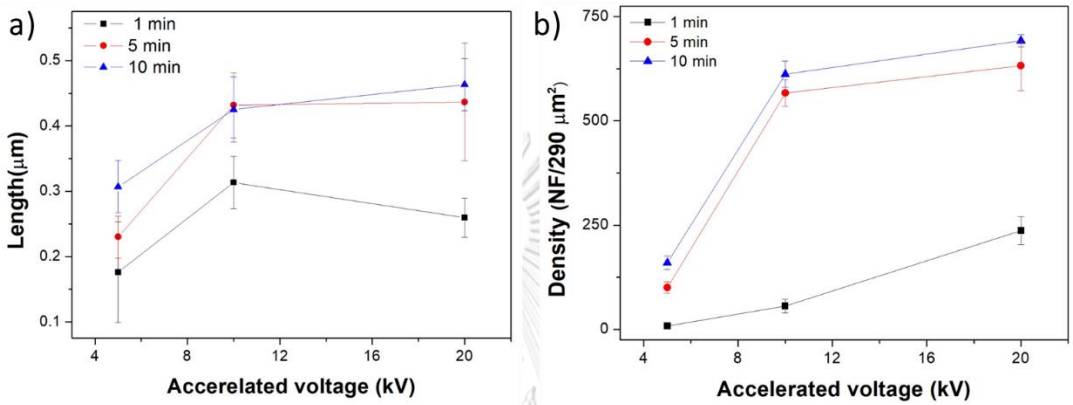

Figure 4.26 a) The density of Ag NFs and b) the length of Ag NFs as a function of the irradiation time.

The mechanism of Ag NF fabrication can be divided into four steps and described in Figure 4.27 The first step was the heat generation when an electron beam was irradiated on Ag_2S surface. With the lower accelerated voltage, the lower kinetic energy electrons were produced, then a number of **β**-Ag_2S nuclei were formed. With the higher voltage used, a greater number of the higher kinetic energy electrons were generated leading to the phase transformation of **α**-Ag_2S to **β**-Ag_2S and causing a large number of **β**-Ag_2S nuclei formation on the Ag_2S surface. The second step was related to the diffusion of the Ag^+ ions inside the lattice of **β**-Ag_2S to the surface of **β**-Ag_2S. These Ag^+ ions on the surface could react with the electrons from the electron irradiation and were reduced to Ag. The Ag islands were then formed by the reduction of Ag^+ ions to Ag at the hexagonal side which has the minimal lattice mismatch with Ag (111). The different amount of **β**-Ag_2S led to the different density of Ag islands and the density of Ag islands could be saturated due to the limitation of **β**-Ag_2S. So the accelerated voltage was found to be the dominant parameter on the first and second

steps. Moreover, the reduction of Ag^+ ion induced on Ag_2S surface. In the third step, due to the charge inducing, the oxidation of Ag thin film was occurred. Ag^+ ions can act as Ag backup for increasing length of Ag islands due to the Ag^+ ion reduction. The energy barrier of Ag^+ ion jumping for accept e^- is 89 meV. The longer irradiation time was used to irradiate on Ag_2S surface, the longer Ag NFs were obtained. In the last step, when Ag backup was depleted the length of Ag NFs was saturated. So the irradiation time was found to be the dominant parameter in step 3 and 4.

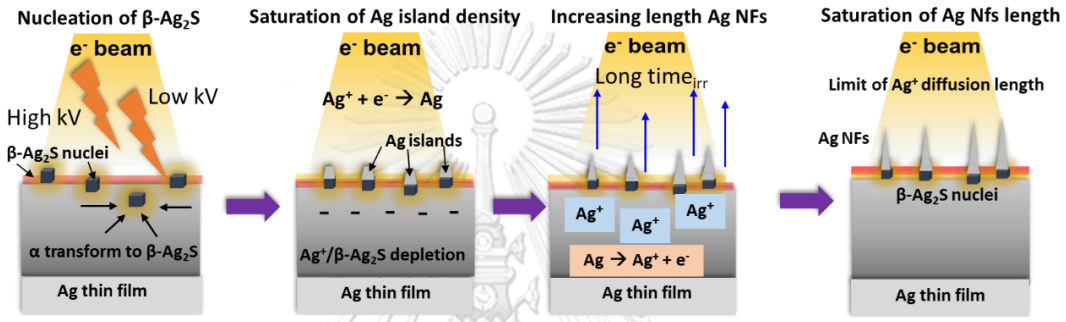

Figure 4. 27. Mechanism of Ag NFs growth

4.4. SERS activity test

After the electron irradiation, we demonstrate the utilization of Ag NFs SERS substrate. MB at the concentration of $1x10^{-3}$ M was used to observe the enhancement effect of the fabricated SERS substrate via Raman spectroscopy as shown in Figure 4.27. The peak at 521 cm^{-1} corresponds to the Raman scattering of the crystalline Si substrate. The Raman shift at 1623 cm^{-1} is the characteristic peak of MB. The Raman spectra show that the peak intensity of MB at 1623 cm^{-1} on Ag NFs grown on Ag_2S (SERS substrate) by using 20 kV of accelerated voltage and 10 min of irradiation time. Ag NFS SERS substrate was enhanced when compared to those on the commercial SERS and Ag from sputtering. The enhancement factor (EF) was calculated to compare the enhancement effect between Si substrate and Ag NFs SERS substrate (equation 2) [6] . The calculation is show in appendix

$$EF = \frac{I_{SERS}}{I_{Ref}} \times \frac{N_{Ref}}{N_{SERS}} \qquad (2)$$

I_{SERS}: The enhance intensity of adsorbed MB molecules on SERS substrate

I_{Ref}: The spontaneous Raman scattering intensity from bulk MB molecules under the laser spot on the blank Si substrate.

N_{SERS}: The number of MB molecules uniformly spreading on the SERS substrate under the laser spot.

N_{Ref}: The number of the bulk MB molecules excited by the laser without Raman enhance effect

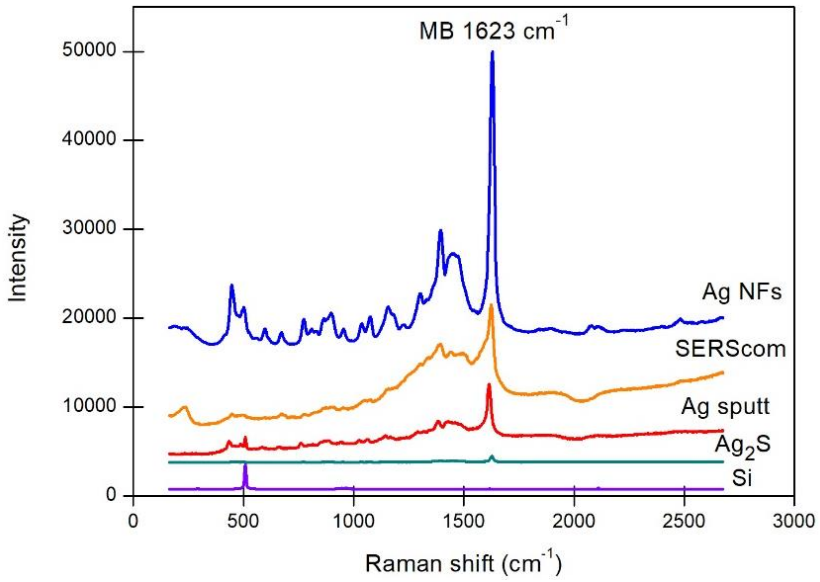

Figure 4.28 Raman spectra of methylene blue (MB) at a concentration of 10^{-3} M on Si, Ag_2S, Ag from sputtering technique and Ag NFs SERS substrates

The EF of Ag NFs SERS substrate was achieved at 1.57×10^6 which is 2 orders of magnitude higher than that of Ag from sputtering (2.05×10^4). This result indicates that the highest density of Ag NFs plays an important role in surface plasmon resonance (SPR). The greater enhancement is observed when the SPR wavelength of Ag NFs matches with the wavelength of the excitation laser. Moreover, the limit of detection was found at 10 nM of MB concentration as shown in Figure 4.28. Moreover, the SERS activity of Ag_{elec} was also shown in appendix. This result can confirm that the Ag NFs

has the properties to enhance the Raman signal via SPR effect with the optimum condition for e^- irradiation of 20 kV accelerated voltage and 10 min irradiation time.

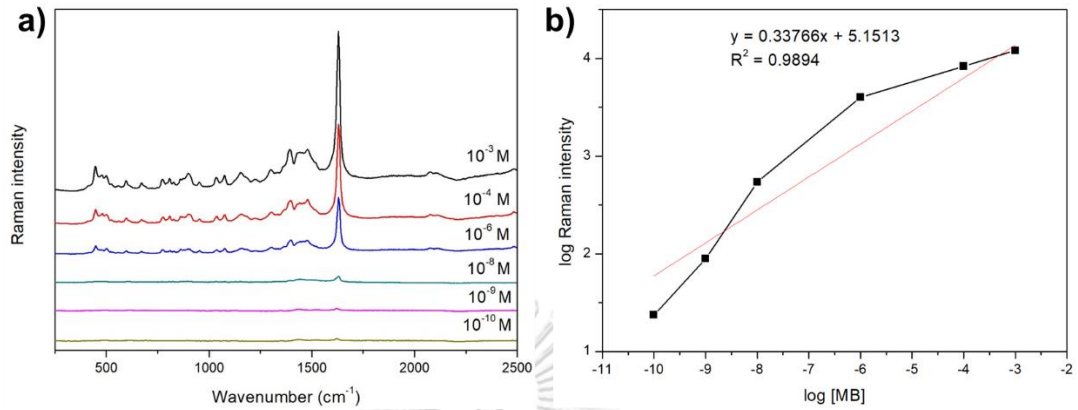

Figure 4.29 a) A comparison of Raman spectra of different concentrations of MB and b) the linear plot between log[MB] and logarithmic function of the Raman intensity.

4.5. Fabrication of Ag NF tip

The Ag tip was prepared from RF magnetron sputtering technique with the same condition from the section 4.1. After that, the Ag_2S tip was prepared by dipping Ag tip into 0.5 Na_2S solution for 6 h of dipping time. The Si, Ag and Ag_2S tips were characterized by SEM and EDS as shown in Figure 4.29.

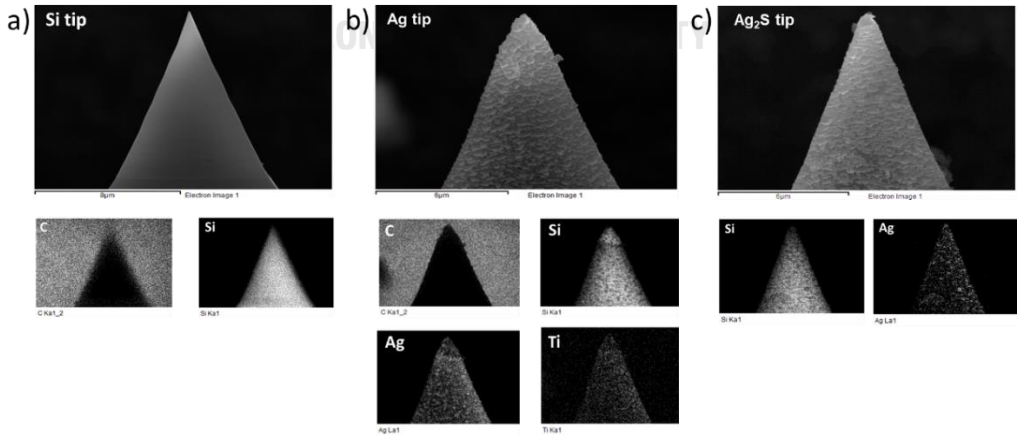

Figure 4.30 The SEM images and EDS mapping of a) Si tip, b) Ag tip and c) Ag_2S tip.

After that, Ag_2S tip was irradiated by 20 kV of accelerated voltage for 10 min of irradiation time as shown in Figure 4.30. The SEM images show that the Ag NFs could not be fabricated on the Ag_2S tip apex. It was found that the percentage of Ag deposition on tip apex was decreased from the initial thickness monitor as shown in Figure 4.31. The slope area of tip apex was measured by ImageJ program then the thickness was calculated. The result shows that the thickness of tip apex is 0.098 μm which was equal to 49.1% of the Ag deposition from thickness monitor. So the thickness of initial Ag from sputtering was increased to 400 nm.

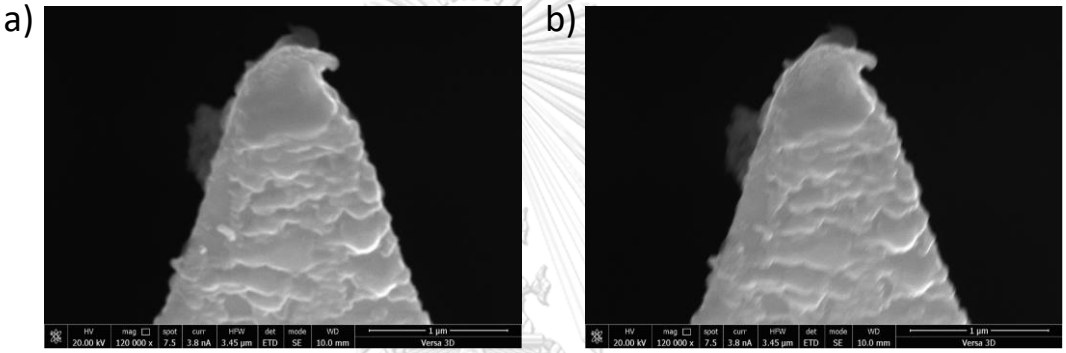

Figure 4.31 The SEM images of Ag_2S tip after irradiation a) 1 min and b) 10 min with 20 kV of accelerated voltage. Ag_2S tip was prepared by dipping Ag tip into 0.5 Na_2S solution for 6 h.

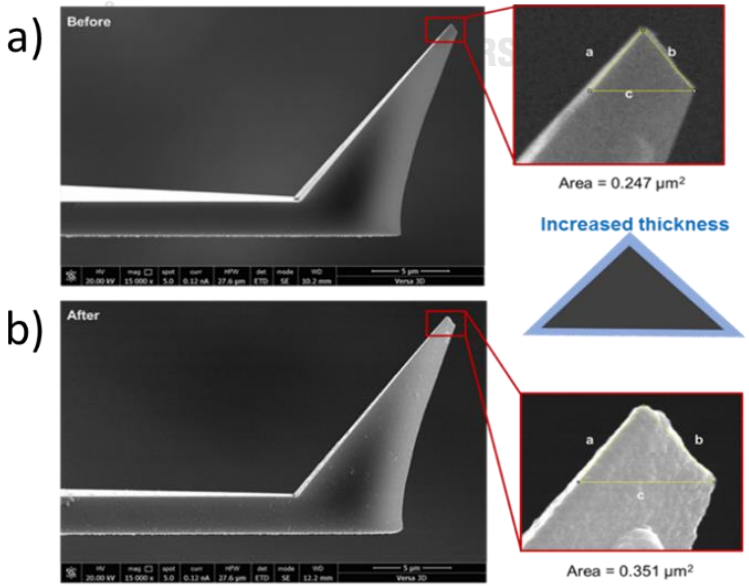

Figure 4.32 The SEM images of AFM tip a) before and b) after Ag sputtering

After increasing Ag thickness on the AFM tip to four-times more than on the substrate, the Ag_2S tip was fabricated with the same condition of Ag_2S thin film and irradiated by 20 kV of accelerated voltage for 10 min of irradiation time as shown in Figure 4.32.

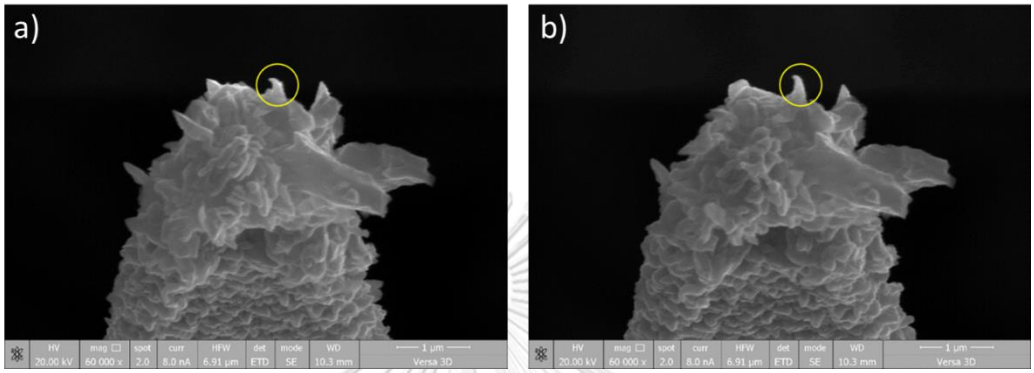

Figure 4.33 The SEM images of Ag_2S tip (4x) after irradiation for a) 1 min and b) 10 min with 20 kV of accelerated voltage. Ag_2S tip was prepared by dipping Ag tip into 0.5 Na2S solution for 6 h.

The SEM images in Figure 4.32 show that the Ag NFs was formed on the Ag_2S tip apex after irradiation for 10 min. This indicates that the initial thickness of Ag has an effect on Ag NFs fabrication via the electron irradiation. The formation of Ag NFs was confirmed by EDS mapping as shown in Figure 4.33. This result shows the Ag mapping of the Ag NFs at the tip apex.

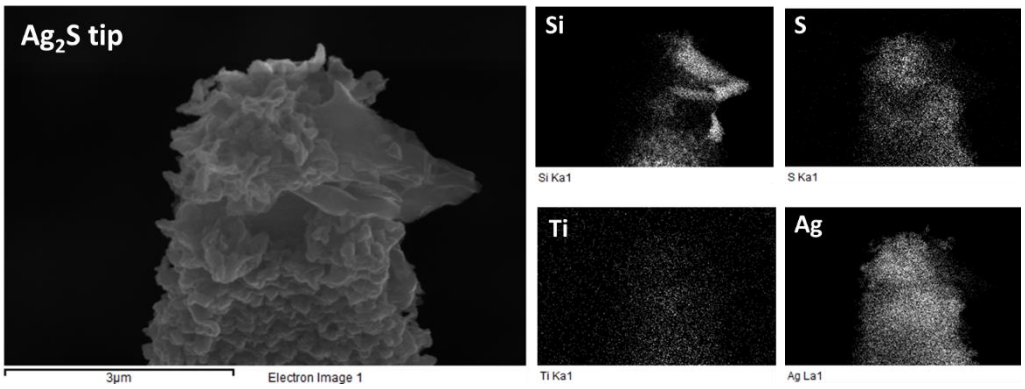

Figure 4.34 The SEM image and EDS mapping of Ag_2S tip with Ag NFs on the tip apex.

4.6. TERS performance measurement

Due to the problem of AFM-Raman spectroscopy, we cannot measure the TERS activity of Ag NFs tip. The Ag NFs tip was separately measured the performance in terms of morphology and the enhancement of Raman signal. The Ag NF tip was used as an AFM tip for scanning the grating compared to the normal Si AFM tip as shown in Figure 4.34. The AFM image obtained from Ag NF tip show that the morphology of grating was slightly different from that obtained from Si tip resulting from the blunter of the tip and softer of Ag NFs on the Ag_2S tip apex.

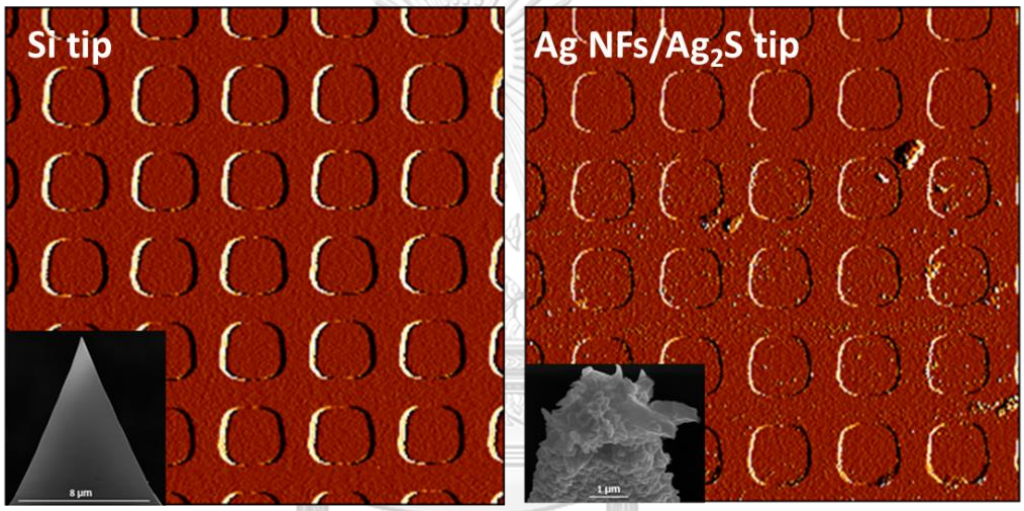

Figure 4.35 The comparison of AFM images scanned by Si tip and Ag NFs tip on the grating surface.

Then, Ag NFs tip was tested for the Raman enhancement by using Ag NFs tip as a SERS substrate. From Figure 4.35, Raman signal of 10^{-3} mM MB on the Ag NFs tip shows higher enhancement than hat on Si tip. The EF of Ag NFs Tip as the SERS substrate was achieved at 4.27×10^{4}. This indicates that the Ag NFs tip plays an important role in surface plasmon resonance (SPR).

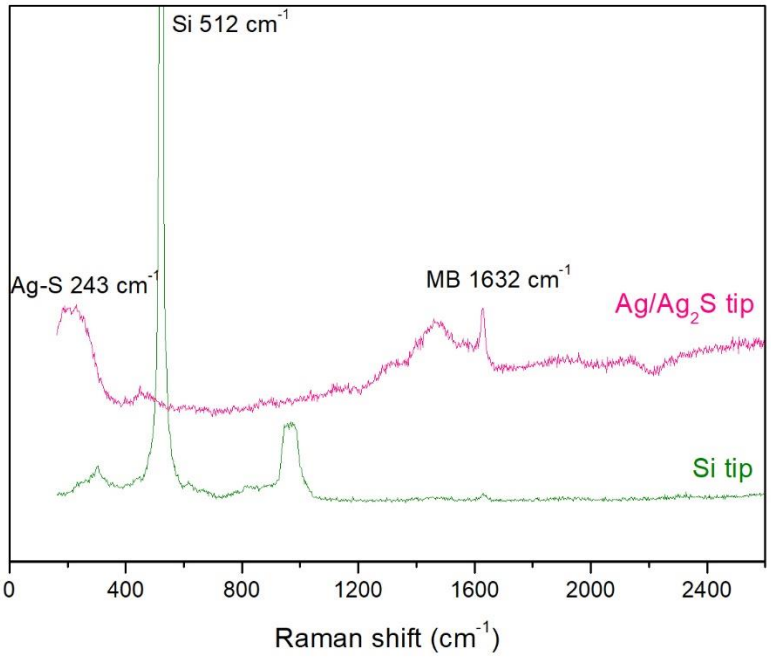

Figure 4.36 Raman spectra of methylene blue (MB) at a concentration of 10^{-3} M on Si and Ag NFs tip as SERS substrates

CHAPTER V

CONCLUSIONS

The Ag NFs fabrication based on β-Ag_2S solid electrolyte have been accomplished. The Ag NFs gave the high sensitivity SERS substrate via the electron irradiation of β-Ag_2S solid electrolyte. The optimum condition for β-Ag_2S fabrication was found to be at 0.5 mM Na_2S for 6 h with pH 8.45 by chemical bath deposition (CBD). β-Ag_2S play a critical role and directly affect the Ag NFs formation. Moreover, heat is the essential parameter for Ag NFs fabrication. The highest density and length were achieved from 20 kV of accelerated voltage and 10 minutes of irradiation time by electron beam irradiation. The highest density and length of Ag NFs were found to be 5.93 x 10^9 NF/cm^2 and 0.46 ± 0.04 μm, respectively. The Ag NFs performance has been investigated by using Ag NFs as SERS substrates. Methylene blue (MB) adsorbed on Ag NFs substrate with green laser (532 nm) and the maximum SERS enhancement factor of 1.57x10^6 was achieved. The limit of detection of MB obtained from Ag NFs substrate was found to be at 10 nM. The highest enhancement factor of 4.27 x 10^4 of MB absorb on Ag NFs TERS tip performed as SERS substrate was achieved.

APPENDIX

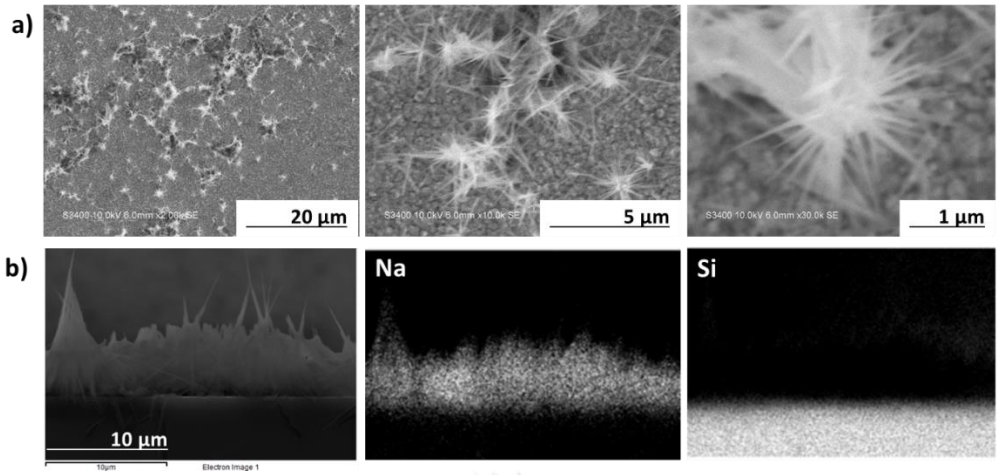

Figure A.1 a) The SEM image of Na growth on Ag_{elec} thin film with different magnifications, b) EDS mapping of elements on the surface of Ag_{elec} prepared from potentiosatat.

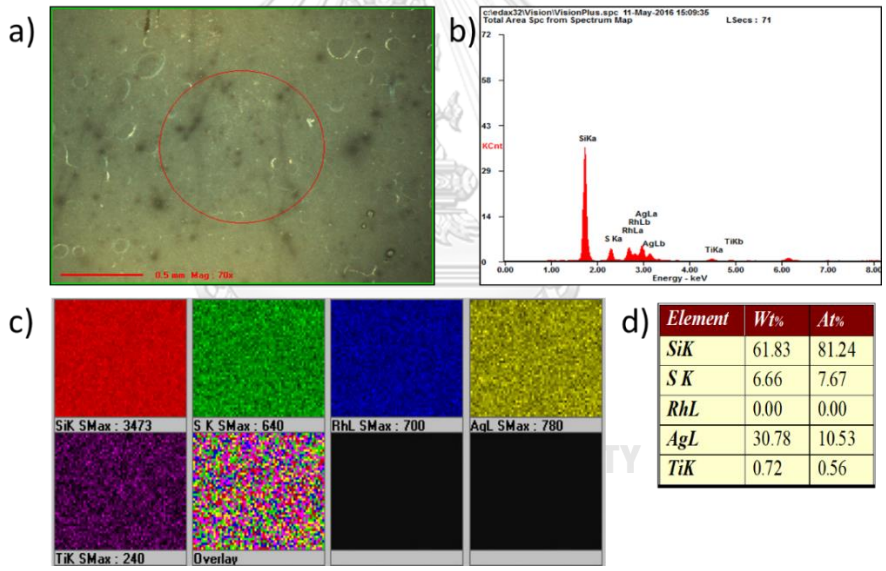

Element	Wt%	At%
SiK	61.83	81.24
S K	6.66	7.67
RhL	0.00	0.00
AgL	30.78	10.53
TiK	0.72	0.56

Figure A.2 a) The optical image, b) XRF spectrum of elements, c) elemental mappings, and d) percentage of each element in the area on the surface of Ag_2S prepared from 2 mM Na_2S solution and 100 nm of Ag thin film.

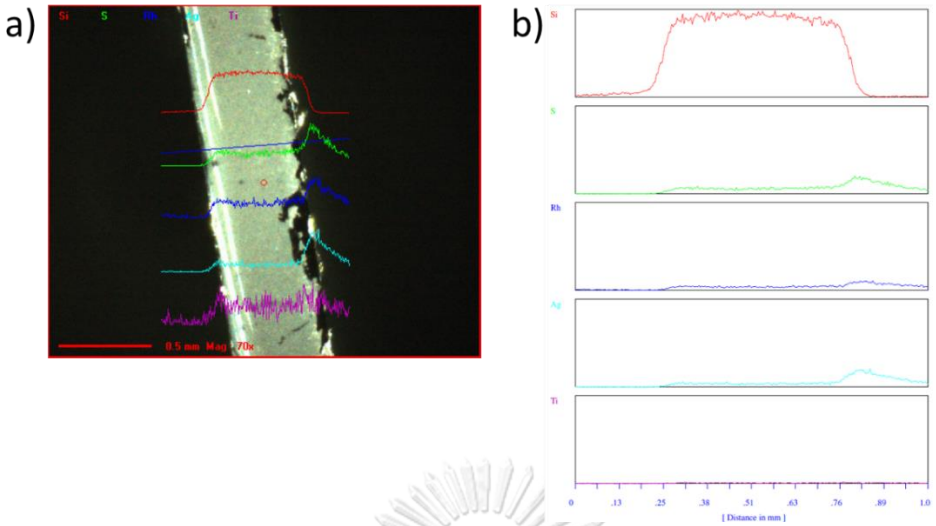

Figure A.3 a) The optical images and the cross line and b) the corresponding integral intensity of each element on the surface of Ag_2S thin film prepared from 2 mM Na_2S solution and 100 nm of Ag thin film.

The Enhancement calculation

$$EF = \frac{I_{SERS}}{I_{Ref}} \times \frac{N_{Ref}}{N_{SERS}} \qquad (2)$$

I_{SERS}: The enhance intensity of adsorbed MB molecules on SERS substrate

I_{Ref}: The spontaneous Raman scattering intensity from bulk MB molecules under the laser spot on the blank Si substrate.

N_{SERS}: The number of MB molecules uniformly spreading on the SERS substrate under the laser spot.

$$\frac{(laser\ spot\ size)^2}{(MB\ space)^2}$$

N_{Ref}: The number of the bulk MB molecules excited by the laser without Raman enhance effect

$$\frac{[MB]x\ 6.02x10^{23}x\ V_{MB}}{\pi r^2}$$

Example

$$EF_{Ag\ NFs} = \frac{(31524)}{16} \times \frac{(0.000001\ m)^2/(2\times10^{-9}\ m)^2}{\left(1\times10^{-3}\frac{mol}{L}\right)\times(6.02\times10^{23})\times(3\times10^{-6}\ L)/(3.14)\times(0.0015\ m)^2}$$

$$= 2.01 \times 10^6$$

REFERENCES

[1] Allu, A.R., et al. Understanding the Formation of CaAl2Si2O8 in Melilite-Based Glass-Ceramics: Combined Diffraction and Spectroscopic Studies. ACS Omega 2(9) (2017): 6233-6243.

[2] Dolui, S., Roy, A., Pal, U., Saha, A., and Maiti, N.C. Structural Insight of Amyloidogenic Intermediates of Human Insulin. ACS Omega 3(2) (2018): 2452-2462.

[3] Sambalova, O., et al. Carboxylate Functional Groups Mediate Interaction with Silver Nanoparticles in Biofilm Matrix. ACS Omega 3(1) (2018): 724-733.

[4] Chen, L., Gao, Y., Xu, H., Wang, Z., Li, Z., and Zhang, R.-Q. The mechanism of N-Ag bonding determined tunability of surface-enhanced Raman scattering of pyridine on MAg (M = Cu, Ag, Au) diatomic clusters. Physical Chemistry Chemical Physics 16(38) (2014): 20665-20671.

[5] Gong, X., Bao, Y., Qiu, C., and Jiang, C. Individual nanostructured materials: fabrication and surface-enhanced Raman scattering. Chemical Communications 48(56) (2012): 7003-7018.

[6] Le Ru, E.C. and Etchegoin, P.G. Quantifying SERS enhancements. MRS Bulletin 38(08) (2013): 631-640.

[7] Zhang, X., Young, M.A., Lyandres, O., and Van Duyne, R.P. Rapid Detection of an Anthrax Biomarker by Surface-Enhanced Raman Spectroscopy. Journal of the American Chemical Society 127(12) (2005): 4484-4489.

[8] Reguera, J., Langer, J., Jimenez de Aberasturi, D., and Liz-Marzan, L.M. Anisotropic metal nanoparticles for surface enhanced Raman scattering. Chem Soc Rev 46(13) (2017): 3866-3885.

[9] Wang, H., Jiang, X., Lee, S.T., and He, Y. Silicon nanohybrid-based surface-enhanced Raman scattering sensors. Small 10(22) (2014): 4455-68.

[10] Clark, A.W. and Cooper, J.M. Nanogap ring antennae as plasmonically coupled SERRS substrates. Small 7(1) (2011): 119-25.

[11] Muniz-Miranda, M., Gellini, C., and Giorgetti, E. Surface-Enhanced Raman Scattering from Copper Nanoparticles Obtained by Laser Ablation. The Journal of Physical Chemistry C 115(12) (2011): 5021-5027.

[12] <Ultrahigh-Density Array of Silver Nanoclusters for SERS Substrate with High Sensitivity and Excellent Reproducibility.pdf>.

[13] Fan, M., Andrade, G.F., and Brolo, A.G. A review on the fabrication of substrates for surface enhanced Raman spectroscopy and their applications in analytical chemistry. Anal Chim Acta 693(1-2) (2011): 7-25.

[14] Fateixa, S., Nogueira, H.I., and Trindade, T. Hybrid nanostructures for SERS: materials development and chemical detection. Phys Chem Chem Phys 17(33) (2015): 21046-71.

[15] McNay, G., Eustace, D., Smith, W.E., Faulds, K., and Graham, D. Surface-enhanced Raman scattering (SERS) and surface-enhanced resonance Raman scattering (SERRS): a review of applications. Appl Spectrosc 65(8) (2011): 825-37.

[16] Sharma, B., et al. High-performance SERS substrates: Advances and challenges. MRS Bulletin 38(08) (2013): 615-624.

[17] Pettinger, B., Schambach, P., Villagomez, C.J., and Scott, N. Tip-enhanced Raman spectroscopy: near-fields acting on a few molecules. Annu Rev Phys Chem 63 (2012): 379-99.

[18] Schmid, T., Opilik, L., Blum, C., and Zenobi, R. Nanoscale chemical imaging using tip-enhanced Raman spectroscopy: a critical review. Angew Chem Int Ed Engl 52(23) (2013): 5940-54.

[19] Stöckle, R.M., Suh, Y.D., Deckert, V., and Zenobi, R. Nanoscale chemical analysis by tip-enhanced Raman spectroscopy. Chemical Physics Letters 318(1) (2000): 131-136.

[20] Willets, K.A. and Van Duyne, R.P. Localized Surface Plasmon Resonance Spectroscopy and Sensing. Annual Review of Physical Chemistry 58(1) (2007): 267-297.

[21] Kumar, N., Mignuzzi, S., Su, W., and Roy, D. Tip-enhanced Raman spectroscopy: principles and applications. EPJ Techniques and Instrumentation 2(1) (2015): 9.

[22] Verma, P. Tip-Enhanced Raman Spectroscopy: Technique and Recent Advances. Vol. 117, 2017.

[23] Meng, L., Huang, T., Wang, X., Chen, S., Yang, Z., and Ren, B. Gold-coated AFM tips for tip-enhanced Raman spectroscopy: theoretical calculation and experimental demonstration. Optics Express 23(11) (2015): 13804-13813.

[24] Gao, L., Zhao, H., Li, T., Huo, P., Chen, D., and Liu, B. Atomic Force Microscopy Based Tip-Enhanced Raman Spectroscopy in Biology. Int J Mol Sci 19(4) (2018).

[25] Huang, T.X., et al. Rational fabrication of silver-coated AFM TERS tips with a high enhancement and long lifetime. Nanoscale 10(9) (2018): 4398-4405.

[26] Williams, C. and Roy, D. Fabrication of gold tips suitable for tip-enhanced Raman spectroscopy. Vol. 26, 2008.

[27] Pozzi, E.A., et al. Ultrahigh-Vacuum Tip-Enhanced Raman Spectroscopy. Chem Rev 117(7) (2017): 4961-4982.

[28] Sheng, S., Li, W., Gou, J., Cheng, P., Chen, L., and Wu, K. Low-temperature, ultrahigh-vacuum tip-enhanced Raman spectroscopy combined with molecular beam epitaxy for in situ two-dimensional materials' studies. Review of Scientific Instruments 89(5) (2018).

[29] Nayak, A., et al. Rate-Limiting Processes Determining the Switching Time in a Ag2S Atomic Switch. The Journal of Physical Chemistry Letters 1(3) (2010): 604-608.

[30] Tran, Q.H., Nguyen, V.Q., and Le, A.-T. Silver nanoparticles: synthesis, properties, toxicology, applications and perspectives. Advances in Natural Sciences: Nanoscience and Nanotechnology 4(3) (2013).

[31] Sharma, B., Frontiera, R.R., Henry, A.-I., Ringe, E., and Van Duyne, R.P. SERS: Materials, applications, and the future. Materials Today 15(1-2) (2012): 16-25.

[32] Mosier-Boss, P.A. Review of SERS Substrates for Chemical Sensing. Nanomaterials (Basel) 7(6) (2017).

[33] Meng, L., Sun, M., Chen, J., and Yang, Z. A Nanoplasmonic Strategy for Precision in-situ Measurements of Tip-enhanced Raman and Fluorescence Spectroscopy. Sci Rep 6 (2016): 19558.

[34] Cho, W.J., Kim, Y., and Kim, J.K. Ultrahigh-Density Array of Silver Nanoclusters for SERS Substrate with High Sensitivity and Excellent Reproducibility. ACS Nano 6(1) (2012): 249-255.

[35] Ding, S.-Y., et al. Nanostructure-based plasmon-enhanced Raman spectroscopy for surface analysis of materials. Nature Reviews Materials 1(6) (2016).

[36] Ivanov-Shitz, A.K. Computer simulation of superionic conductors: II. Cationic conductors. Review. Crystallography Reports 52(2) (2007): 302-315.

[37] Lim Wen, P., Zhang, Z., Low Hong, Y., and Chin Wee, S. Preparation of Ag2S Nanocrystals of Predictable Shape and Size. Angewandte Chemie International Edition 43(42) (2004): 5685-5689.

[38] Sadovnikov, S.I., Gusev, A.I., and Rempel, A.A. Nonstoichiometry of nanocrystalline monoclinic silver sulfide. Physical Chemistry Chemical Physics 17(19) (2015): 12466-12471.

[39] Motte, L. and Urban, J. Silver Clusters on Silver Sulfide Nanocrystals: Synthesis and Behavior after Electron Beam Irradiation. The Journal of Physical Chemistry B 109(46) (2005): 21499-21501.

[40] Tanaka, H., Akai, T., Tanaka, D., and Ogawa, T. Sequential Phase Transition during Fabricating ^|^beta;-Ag2S Film on Ag Electrode by Wet Chemical Process. Vol. 12, 2014.

[41] Sadovnikov, S.I., Gusev, A.I., and Rempel, A.A. An in situ high-temperature scanning electron microscopy study of acanthite-argentite phase transformation in nanocrystalline silver sulfide powder. Phys Chem Chem Phys 17(32) (2015): 20495-501.

[42] Tang, A., et al. Controllable synthesis of silver and silver sulfide nanocrystals via selective cleavage of chemical bonds. (1361-6528 (Electronic)).

[43] Terabe, K., Nakayama, T., Hasegawa, T., and Aono, M. Formation and disappearance of a nanoscale silver cluster realized by solid electrochemical reaction. Vol. 91, 2002.

[44] Otto, A. Surface enhanced Raman scattering (SERS), what do we know? Applications of Surface Science 6(3) (1980): 309-355.

[45] Ueba, H., Ichimura, S., and Yamada, H. Where are we in the study of SERS? Role of chemisorption and charge transfer. Surface Science 119(2) (1982): 433-448.

[46] Huang, T.-X., Huang, S.-C., Li, M.-H., Zeng, Z., Wang, X., and Ren, B. Tip-enhanced Raman spectroscopy: tip-related issues. Vol. 407, 2015.

[47] Iwami, M., Uehara, Y., and Ushioda, S. Preparation of silver tips for scanning tunneling microscopy imaging. Review of Scientific Instruments 69(11) (1998): 4010-4011.

[48] Dickmann, K., Demming, F., and Jersch, J. New etching procedure for silver scanning tunneling microscopy tips. Review of Scientific Instruments 67(3) (1996): 845-846.

[49] Johnson, T.W., et al. Highly Reproducible Near-Field Optical Imaging with Sub-20-nm Resolution Based on Template-Stripped Gold Pyramids. ACS Nano 6(10) (2012): 9168-9174.

[50] Deckert, V., et al. Spatial resolution in Raman spectroscopy. Faraday Discussions 177(0) (2015): 9-20.

[51] Sadovnikov, S.I. and Gusev, A.I. Facile synthesis, structure, and properties of Ag2S/Ag heteronanostructure. Journal of Nanoparticle Research 18(9) (2016).

[52] Filipič, G. and Cvelbar, U. Copper oxide nanowires: A review of growth. Vol. 23, 2012.

[53] Xu, Z., Bando, Y., Wang, W., Bai, X., and Golberg, D. Real-Time In Situ HRTEM-Resolved Resistance Switching of Ag_2S Nanoscale Ionic Conductor. ACS Nano 4(5) (2010): 2515-2522.

[54] Gusev, A.I. and Sadovnikov, S.I. Acanthite–argentite transformation in nanocrystalline silver sulfide and the Ag_2S/Ag nanoheterostructure. Semiconductors 50(5) (2016): 682-68

VITA

Miss Phichaya Fueaimi was born on April 5, 1992 in Prachinburi, Thailand. She got a high school diploma from Prachinratsadorn Amroong School (Science Mathematic and Technology Program; SMAT) in 2009. From there on, she has obtained the scholarship from the Research Professional Development Project under Science Achievement Scholarship of Thailand (SAST), under office of the Higher Education Commission (OHEC), Ministry of Education Thailand since 2010 until 2014. And then, she graduated and received her Bachelor's degree of Science in Chemistry from Burapha University, Chonburi in 2014. Afterwards, she has pursued Master's degree in Chemistry at Chulalongkorn University. She has become a member of supramolecular research unit and worked under supervision of Dr. Pannee Leeladee and Prof. Dr. Thawatchai Tuntulani. Furthermore, she got the Research grant from The 90th Anniversary of Chulalongkorn University Scholarship. Moreover, she gained the opportunity from using characterized instruments relevant to her research at National Nanotechnology Center (NANOTEC). And she also has obtained the scholarship from Thailand Graduate Institute of Science and Technology (TGIST) under office of the National Science and Technology Development Agency (NSTDA).

Presentation: 2018 Oral presentation of title "Role of β-silver sulfide solid electrolyte on Ag nanofilament fabrication for surface- enhanced Raman spectroscopy activity" The Pure and Applied Chemistry International Conference 2018 (PACCON 2018) (Proceeding).

2017 Poster presentation of title "Fabrication of silver nano-protrusion based on silver sulfide solid electrolyte for surface-enhanced Raman spectroscopy" The 5th Thailand International Nanotechnology Conference.

Award: Best of the Best Poster Presentation Award, "Fabrication of silver nano-protrusion based on silver sulfide solid electrolyte for surface-enhanced Raman spectroscopy" The 5th Thailand International Nanotechnology Conference.